

An Overview of Low-Rank Structures in the Training and Adaptation of Large Models*

Laura Balzano¹, Tianjiao Ding², Benjamin D. Haeffele², Soo Min Kwon¹, Qing Qu¹, Peng Wang¹, Zhangyang Wang³, and Can Yaras¹

¹ Department of Electrical Engineering and Computer Science, University of Michigan

² University of Pennsylvania

³ Department of Electrical and Computer Engineering, University of Texas at Austin

March 26, 2025

Abstract

The rise of deep learning has revolutionized data processing and prediction in signal processing and machine learning, yet the substantial computational demands of training and deploying modern large-scale deep models present significant challenges, including high computational costs and energy consumption. Recent research has uncovered a widespread phenomenon in deep networks: the emergence of low-rank structures in weight matrices and learned representations during training. These implicit low-dimensional patterns provide valuable insights for improving the efficiency of training and fine-tuning large-scale models. Practical techniques inspired by this phenomenon—such as low-rank adaptation (LoRA) and training—enable significant reductions in computational cost while preserving model performance. In this paper, we present a comprehensive review of recent advances in exploiting low-rank structures for deep learning and shed light on their mathematical foundations. Mathematically, we present two complementary perspectives on understanding the low-rankness in deep networks: (i) the emergence of low-rank structures throughout the whole optimization dynamics of gradient and (ii) the implicit regularization effects that induce such low-rank structures at convergence. From a practical standpoint, studying the low-rank learning dynamics of gradient descent offers a mathematical foundation for understanding the effectiveness of LoRA in fine-tuning large-scale models and inspires parameter-efficient low-rank training strategies. Furthermore, the implicit low-rank regularization effect helps explain the success of various masked training approaches in deep neural networks, ranging from dropout to masked self-supervised learning. In summary, this tutorial provides researchers and practitioners with a deeper understanding of low-rank structures in the training and adaptation of large-scale deep learning models, highlighting both the theoretical foundations and practical applications of low-rank methods, and outlining promising directions for future research.

Key words: deep learning, low-rank adaptation, low-rank training, masked training, efficiency, learning dynamics

*Authors are listed alphabetically. Corresponding authors: Laura Balzano (girasole@umich.edu), Peng Wang (peng8wang@gmail.com), Tianjiao Ding (tjding@upenn.edu).

Contents

1	Introduction	2
2	Background	4
2.1	Deep Artificial Neural Networks	4
2.2	Low-Rank Structure in Data Matrices	5
2.3	Implicit Low-Rank Structures	6
3	Low-Rank Structure at Every Iteration of Gradient Dynamics	7
3.1	Analysis of Training Dynamics	7
3.2	Low-Rank Adaptation for Fine-tuning Large-Scale Models	10
3.2.1	Choosing the Learning Rate	11
3.2.2	Choosing the Rank Allocation	12
3.3	Low-Rank Training	13
4	Low-Rank Structure at the Convergence of Gradient Methods	15
4.1	Implicit Regularization	15
4.2	Low-Rank from l_2 Regularization	15
4.3	Low-Rank Structure from Implicit Regularization	17
4.4	Masked Training	18
5	Open Questions and Future Directions	20
A	Experiment Details	24
B	Complexity for Forward and Backward Pass	24
C	Low-Rank Gradient Dynamics with a Wide Target	25
D	Low-Rank Training	25

1 Introduction

The advent of deep learning and large-scale computing has immeasurably changed the ways we process, interpret, and predict data in signal processing and machine learning. However, training and deploying modern deep learning models demand substantial computational resources, raising concerns about exorbitant training costs, GPU shortages, and heightened energy consumption in the coming years. Additionally, our theoretical understanding of how deep learning works is limited compared to that of classical signal processing methods. As a concrete example, classical wisdom in signal processing and statistical inference suggests that the number of data samples we use for parameter estimation should be comparable or larger than the number of parameters in a model for the learning to be accurate and sample-efficient. Yet, this is not the case for most state-of-the-art deep learning models, where the number of parameters often far exceeds the available data samples.

Within the general study of the mathematics of deep learning, several lines of research over the last decade have explored the emergence of low-dimensional structures during the training process, where basic elements such as weight matrices and representations (e.g., outputs of certain layers of a neural network) tend to be approximately low-rank even though not explicitly trained to be. These low-dimensional structures arise in part due to implicit bias of the methods used to train deep networks, providing the potential to partially explain why deep models need fewer samples than the number of model parameters. This implicit low-dimensionality has inspired the exploration of low-rank structures in training and fine-tuning large-scale deep learning models more efficiently. For example, low-rank adaptation (LoRA) [2], which adds a

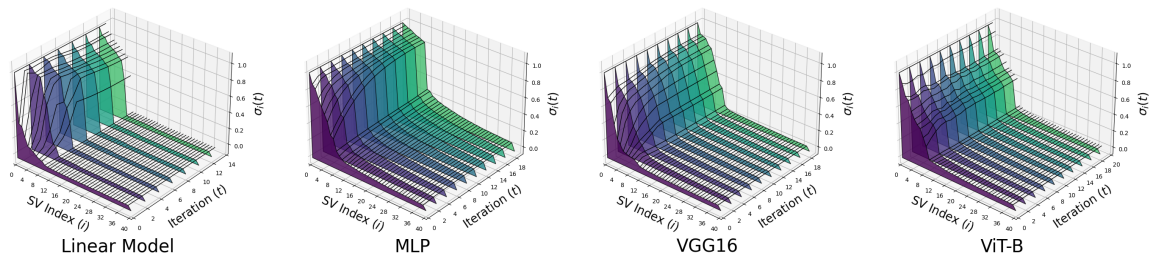


Figure 1: Prevalence of low-rank weight updates in various deep networks. Each plot visualizes the singular values of the weight updates from initialization for the penultimate layer weight matrix for different types of network architectures: deep linear network (DLN), multi-layer perceptron (MLP), VGG, and ViT-B. The linear network is trained on MNIST with mean square error loss. The MLP is trained on MNIST with cross-entropy loss. The VGG and ViT-B networks are both trained on CIFAR-10 with cross-entropy loss. The result shows a prevalent phenomenon across linear and nonlinear networks – gradient descent only updates a small portion of the singular values, while the others remain small and almost unchanged. Figure courtesy of [1].

low-rank factorized update to the weight matrices for model fine-tuning using much-reduced computation and memory. It has gained significant attention in the past few years due to its impressive performance in fine-tuning large language models (LLMs), vision-language models, and image generation models. Inspired by this success, deep learning practitioners further explicitly factorize weight matrices into low-rank factors for post-training compression, as well as training low-rank models from scratch, with promising results. For instance, recent advances made by the DeepSeek-V3 model [3] have achieved impressive language generation results with significantly compressed model size, in part by using a low-rank factorization of the query matrices in the multi-head attention during training and inference. In this paper, we review recent exciting advances and aim to clarify the mathematical foundations underlying their design. Specifically, we highlight key insights from a rich line of research focused on theoretically understanding and leveraging low-rank structures in deep learning.

Structure in optimization dynamics vs. implicit regularization of the objective. We will examine low-rank structures that emerge during the training of deep networks. While these structures have been explored extensively in the literature, we adopt two distinct perspectives. The first perspective focuses on the low-rank structure present throughout the iteration of the learning dynamics. The second perspective investigates how the optimization objective function itself implicitly induces such structures.

- **Structure in Optimization Dynamics (Section 3):** From this perspective, we aim to show that the dynamics of some iterative optimization algorithm applied to a particular problem have a given structure at every iteration. This structure could then be exploited throughout the entire optimization process to reduce the computation and memory cost; see Figure 1 for an illustration.
- **Structure at Convergence (Section 4):** From this perspective, we aim to show that while a given objective function may not have directly been designed to impose a particular structure through regularization, still the final solution may be constrained to have low-rank structure. As illustrated in Figure 2, we are able to show the equivalence of the given objective to another regularized objective function, and characterize the structure of the solution at convergence of the algorithm, as opposed to at every iteration.

Paper Organization. In Section 2, we review the mathematical foundations of the low-rank learning dynamics in training these models under simplified models, which provide insights into low-rank adaptation and training methods. In Section 3.1, we analyze low-rank structure arising in the training dynamics of deep linear networks. In Section 3.2, we leverage these insights for understanding the LoRA method and its variants. Then we will survey recent low-rank training methods in Section 3.3. In Section 4, we discuss low-rank structure emerging at the convergence of training algorithms. Finally, we will conclude by discussing open questions in Section 5.

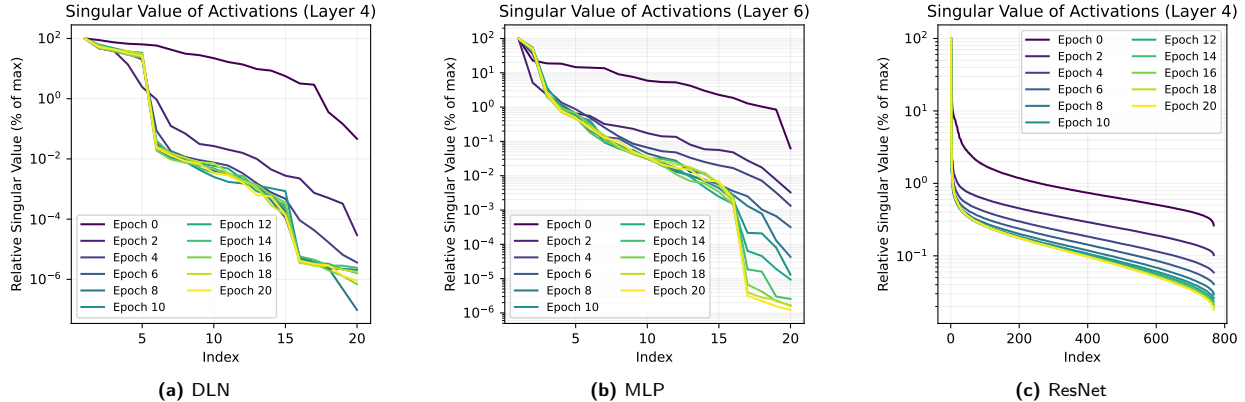


Figure 2: Singular values of activations of the last layer in deep architectures trained with dropout rate 60%, as a function of training epoch. Deep Linear Network (DLN) and Multi-Layer Perceptron (MLP) are trained on synthetic data with MSE loss, while ResNet is trained on CIFAR-10 dataset of natural images with cross-entropy loss. Notably, the activations of the layer gradually become low-rank as masked training proceeds.

2 Background

2.1 Deep Artificial Neural Networks

In this section, we formally introduce the basic setup of deep artificial neural networks. Mathematically, an artificial neural network can be represented as a function $f_{\Theta} : \mathbb{R}^d \rightarrow \mathbb{R}^k$ that maps input data to an output space, where Θ denotes the network or function parameters. Those parameters are set through the learning or training process. Suppose that we have training data samples $\{(x_i, y_i)\} \subseteq \mathbb{R}^d \times \mathbb{R}^k$, where $x_i \in \mathbb{R}^d$ denotes the i -th input and $y_i \in \mathbb{R}^k$ is an associated label or target output prediction. To learn the network parameters, one can minimize the empirical risk over the training samples:

$$\min_{\Theta} F(\Theta) := \sum_{i=1}^n \mathcal{L}(f_{\Theta}(x_i), y_i) + \lambda \mathcal{R}(\Theta), \quad (1)$$

where n denotes the number of training samples, $\mathcal{L} : \mathbb{R}^k \times \mathbb{R}^k \rightarrow \mathbb{R}_+$ is the training loss function, and $\mathcal{R} : \mathbb{R}^k \rightarrow \mathbb{R}$ and $\lambda \geq 0$ denote the regularization function and regularization strength, respectively. Common loss functions for \mathcal{L} include mean-squared error (MSE), cross-entropy (CE), and label smoothing. Much of the deep learning literature focuses on training without explicit regularization (i.e., $\lambda = 0$). Nonetheless, the inherent dynamics of training can still induce implicit regularization, often giving rise to low-rank structures in network parameters, as we will discuss later.

Example 2.1 (Multilayer Perceptron). A simple yet fundamental type of artificial neural network is the multi-layer perceptron (MLP), which is a feedforward neural network composed of multiple layers of neurons and can be mathematically represented as a function $f_{\Theta} : \mathbb{R}^d \rightarrow \mathbb{R}^k$ of the following form:

$$f_{\Theta}(x) = \mathbf{W}_L \sigma(\mathbf{W}_{L-1} \sigma(\dots \sigma(\mathbf{W}_1 x))) , \quad (2)$$

where $\mathbf{W}_l \in \mathbb{R}^{d_l \times d_{l-1}}$ denotes the weight matrix of the l -th layer for each $l \in [L]$ with $d_0 = d$ and $d_L = k$, $\sigma(\cdot)$ is typically¹ an element-wise activation function, such as ReLU, sigmoid, or tanh function [4], and $\Theta = \{\mathbf{W}_l\}_{l=1}^L$ denotes the collection of all trainable network parameters. A deep linear network has this form with $\sigma(\cdot)$ as the identity function, i.e.,

$$f_{\Theta}(x) = \mathbf{W}_L \mathbf{W}_{L-1} \dots \mathbf{W}_1 x. \quad (3)$$

It is worth noting that $f_{\Theta}(\cdot)$ is an end-to-end linear mapping from $x \in \mathbb{R}^d$ to some output in \mathbb{R}^k .

One might ask why learn a deep linear network instead of a single-layer linear mapping, given both represent linear transformations. The reason is that research shows deep, overparameterized linear networks

¹Some MLP architectures have non-element-wise nonlinearities, like layer normalization and max or average pooling.

offer two key benefits: (i) implicit low-rank bias that emerges during the training process and (ii) improved loss landscape that allows for fast convergence. Below in Section 3.1 we will discuss the first point. Moreover, while deep linear networks are primarily of theoretical interest, they have been recognized as valuable prototypes for investigating nonlinear networks due to their simplicity and the resemblance of certain phenomena in their nonlinear counterparts. For example, [5] demonstrated that deep linear networks exhibit a striking hierarchical progressive differentiation of structures in the internal hidden representations, resembling patterns observed in their nonlinear counterparts. To shed light on how deep networks transform inputs into outputs, [6] demonstrated that deep linear networks exhibit layerwise feature compression and discrimination, mirroring the behavior of deep nonlinear networks. Building on these insights, recent research is actively developing tools to extend theoretical findings from linear networks to nonlinear ones, advancing our understanding of underlying principles of deep learning.

2.2 Low-Rank Structure in Data Matrices

This section provides background on low-rank structures in data matrices, a concept widely studied across fields such as signal processing, communications, computer vision, and medical imaging, with applications in signal approximation, direction of arrival estimation, structure-from-motion, and signal reconstruction. Low-rank structure can take many forms, but we focus on the most basic: a linear low-dimensional subspace. When matrix columns lie on (or near) such a subspace, the matrix is exactly (or approximately) low-rank. Other low-dimensional structures, which we do not cover in this tutorial, include unions of low-rank subspaces, low-dimensional manifolds, and algebraic varieties.

A key foundational theorem connecting low-rank factorizations to low-rank approximations of matrices in unitarily invariant norms is as follows.

Theorem 1. *Suppose that $\Phi \in \mathbb{R}^{k \times d}$ admits a singular value decomposition (SVD) $\Phi = U\Sigma V^\top$ with Σ being a diagonal matrix of singular values $\sigma_1 \geq \sigma_2 \cdots \geq \sigma_{\min(k,d)} > 0$. Consider the following optimization problem:*

$$\min_{\mathbf{W}_1 \in \mathbb{R}^{r \times d}, \mathbf{W}_2 \in \mathbb{R}^{k \times r}} \|\mathbf{W}_2 \mathbf{W}_1 - \Phi\|_F^2, \quad (4)$$

where $r \leq \min\{k, d\}$. Any global minimizer $(\mathbf{W}_1, \mathbf{W}_2)$ satisfies $\mathbf{W}_2 \mathbf{W}_1 = \mathbf{U}_r \Sigma_r \mathbf{V}_r^\top$, where Σ_r is a diagonal matrix holding the r largest magnitude singular values of Φ , and $\mathbf{U}_r, \mathbf{V}_r$ hold the corresponding singular vectors². Moreover, the resulting objective value is given by $\|\mathbf{W}_2 \mathbf{W}_1 - \Phi\|_F^2 = \sum_{i=r+1}^{\min(k,d)} \sigma_i^2$.

This result was proved multiple times and is attributed to Schmidt (1907) or Eckart and Young (1936), followed by Mirsky (1960) proving that this minimizer holds for any unitarily invariant norm [7]. A key insight from decades of research is that, despite nonconvexity, many iterative optimization algorithms converge to the minimizer under mild conditions. While SVD provides a solution, it is less adaptable to related but distinct problem formulations.

To connect low-rank structures to deep networks, suppose that we stack our data $\{(\mathbf{x}_i, \mathbf{y}_i)\}_{i=1}^n \subseteq \mathbb{R}^d \times \mathbb{R}^k$ into matrices:

$$\mathbf{X} = [\mathbf{x}_1 \quad \mathbf{x}_2 \quad \cdots \quad \mathbf{x}_n] \in \mathbb{R}^{d \times n}, \quad \mathbf{Y} = [\mathbf{y}_1 \quad \mathbf{y}_2 \quad \cdots \quad \mathbf{y}_n] \in \mathbb{R}^{k \times n}.$$

Using this data matrix and plugging the form of a deep linear network (3) into Problem (1), together with the l_2 norm as the loss function and no regularizer, yields

$$\|\mathbf{W}_L \cdots \mathbf{W}_1 \mathbf{X} - \mathbf{Y}\|_F^2. \quad (5)$$

If we whiten the data by right multiplying \mathbf{X}, \mathbf{Y} with $\mathbf{X}^\top (\mathbf{X} \mathbf{X}^\top)^{-1}$, we have

$$\|\mathbf{W}_L \cdots \mathbf{W}_1 - \mathbf{Y} \mathbf{X}^\top (\mathbf{X} \mathbf{X}^\top)^{-1}\|_F^2. \quad (6)$$

Many papers in this area then consider $\Phi := \mathbf{Y} \mathbf{X}^\top (\mathbf{X} \mathbf{X}^\top)^{-1}$, giving the unconstrained version of (4) for $L = 2$. This assumes that $\mathbf{X} \mathbf{X}^\top$ is invertible, which is usually true when $n > d$, and this is sometimes

²We note for completeness that if the r and $(r+1)$ -st singular values are equal, then these subspaces U_r, V_r are not unique. The singular vectors corresponding to any repeated singular values are unique up to the subspace they span.

described as having an identity input matrix \mathbf{X} . Since the solution for \mathbf{W} when minimizing $\|\mathbf{W}\mathbf{X} - \mathbf{Y}\|_F$ without constraints is simply $\mathbf{W} = \mathbf{Y}\mathbf{X}^\top(\mathbf{X}\mathbf{X}^\top)^{-1}$, these two problems have a close connection.

Based on the above setup, we now discuss two different approaches to inducing low-rank structures in deep linear networks $\mathbf{W}_L \cdots \mathbf{W}_1$ in the context of Problem (6). The first approach explicitly enforces a low-rank constraint on the weight matrices by restricting their rank, such as $\text{rank}(\mathbf{W}_l) \leq r$ with $r < \min\{d_0, \dots, d_L\}$ for each $l \in [L]$. Consequently, Problem (6) can be viewed as a deep low-rank matrix factorization problem. The second approach leverages the low-rank structure of the target matrix Φ . In this case, prior research has shown that gradient descent for training weights exhibits an implicit bias toward learning low-rank solutions, even in the absence of explicit rank constraints. For example, Theorem 2 showed that when Φ is low-rank, each weight matrix is always updated within a low-rank invariant subspace throughout training. Compared to deep linear networks, where low-rank structure is typically imposed on the weight matrices, deep nonlinear networks offer more flexibility in defining and utilizing low-rank structures. This flexibility arises from the various components within nonlinear architectures, such as weight matrices, intermediate output, and optimization dynamics. For example, recent work [1] studied low-rank weight updates of deep nonlinear networks, where only a subset of the top singular values significantly change during weight updates from the initialization of the penultimate layer matrix, i.e., $\mathbf{W}_l^{(t)} - \mathbf{W}_l^{(0)}$; see Figure 1.

2.3 Implicit Low-Rank Structures

Modern deep learning models are often highly underdetermined — containing far more parameters than the number of training samples — yet they demonstrate remarkable generalization to novel data. This phenomenon, known as overparameterization, raises a fundamental question: why do such models generalize well despite their capacity to fit the training data in many different ways? One prominent explanation is that the optimization dynamics used to train overparameterized models inherently favor parsimonious solutions that not only fit the data but also generalize well. This tendency, referred to as *implicit bias* or *implicit regularization*, suggests that common optimization algorithms, such as gradient descent, navigate toward a subset of solutions that avoid overfitting, despite the existence of infinitely many parameter choices that could perfectly fit the training data.

To illustrate this phenomenon, in this section we will show how the gradient dynamics of simple least-squares linear regression constrain the solution (in fact, every iterate of the optimization variable) to lie in a low-dimensional subspace. Suppose we want to predict n scalar outputs $\mathbf{y} = [y_1, \dots, y_n]^\top \in \mathbb{R}^{n \times 1}$ from n, d -dimensional observations $\mathbf{X} = [\mathbf{x}_1, \dots, \mathbf{x}_n]^\top \in \mathbb{R}^{n \times d}$ by finding a coefficient vector $\mathbf{w} \in \mathbb{R}^d$ to solve:

$$\min_{\mathbf{w} \in \mathbb{R}^d} \mathcal{L}(\mathbf{w}) = \frac{1}{2} \|\mathbf{y} - \mathbf{X}\mathbf{w}\|_2^2. \quad (7)$$

Typically one desires $n \geq d$ to ensure a unique solution to this problem. If instead we have fewer measurements than parameters $n < d$, this problem is underdetermined, and there are infinitely many solutions for \mathbf{w} that will result in exactly zero error in this objective function. However, if we optimize with gradient descent, the following equation defines the dynamics of the iterative algorithm:

$$\begin{aligned} \mathbf{w}^{(t)} &= \mathbf{w}^{(t-1)} - \eta \nabla \mathcal{L}(\mathbf{w}) = \mathbf{w}^{(t-1)} - \eta \mathbf{X}^\top (\mathbf{X}\mathbf{w}^{(t-1)} - \mathbf{y}) \\ &= \mathbf{w}^{(t-2)} - \eta \mathbf{X}^\top (\mathbf{X}\mathbf{w}^{(t-2)} - \mathbf{y}) - \eta \mathbf{X}^\top (\mathbf{X}\mathbf{w}^{(t-1)} - \mathbf{y}) \\ &= \dots = \mathbf{w}^{(0)} - \eta \mathbf{X}^\top \sum_{i=0}^{t-1} (\mathbf{X}\mathbf{w}^{(i)} - \mathbf{y}) \end{aligned} \quad (8)$$

Defining $\mathbf{z}^{(t-1)} = \eta \sum_{i=0}^{t-1} (\mathbf{X}\mathbf{w}^{(i)} - \mathbf{y})$, we see that $\mathbf{w}^{(t)} = \mathbf{w}^{(0)} + \mathbf{X}^\top \mathbf{z}^{(t-1)}$. Recall that since $n < d$, \mathbf{X}^\top is a tall matrix; $\mathbf{X}^\top \mathbf{z}$ is in the n -dimensional subspace of \mathbb{R}^d defined by the span of the columns of \mathbf{X}^\top (i.e., the row space of \mathbf{X} , also the orthogonal complement of the nullspace of \mathbf{X}).

This observation leads us to two key points:

1. Every iterate of gradient descent must have the form $\mathbf{w}^{(0)} + \mathbf{X}^\top \mathbf{z}$ for some $\mathbf{z} \in \mathbb{R}^n$. If we initialize with $\mathbf{w}^{(0)} \in \text{rowspan}(\mathbf{X})$ (e.g., $\mathbf{w}^{(0)} = \mathbf{0}$), then every iterate is in the row span of \mathbf{X} . This can be exploited to significantly reduce computation if $n \ll d$ by only optimizing in this subspace.

2. Gradient descent is solving an implicitly constrained problem in place of Equation (7):

$$\min_{\mathbf{u} \in \mathbb{R}^d} \frac{1}{2} \|(\mathbf{y} - \mathbf{X}\mathbf{w}^{(0)}) + \mathbf{X}\mathbf{u}\|_F^2 \quad \text{s.t. } \mathbf{u} \in \text{rowspan}(\mathbf{X}) \subset \mathbb{R}^d \quad (9)$$

or equivalently

$$\min_{\mathbf{z} \in \mathbb{R}^n} \frac{1}{2} \|(\mathbf{y} - \mathbf{X}\mathbf{w}^{(0)}) + \mathbf{X}\mathbf{X}^\top \mathbf{z}\|_F^2. \quad (10)$$

This problem is no longer underdetermined, since $\mathbf{y} - \mathbf{X}\mathbf{w}^{(0)} \in \mathbb{R}^n$ and $\mathbf{X}\mathbf{X}^\top$ is a square $n \times n$ matrix. Again assuming that \mathbf{X} has rank n , the unique minimizer to this convex problem is $\mathbf{z}^* = (\mathbf{X}\mathbf{X}^\top)^{-1}(\mathbf{y} - \mathbf{X}\mathbf{w}^{(0)})$, corresponding to $\mathbf{w}^* = \mathbf{X}\mathbf{z}^*$ in the original problem, and this is the solution at convergence for gradient descent. If we initialize with $\mathbf{w}^{(0)} = 0$, we see that the solution is $\mathbf{w}^* = \mathbf{X}(\mathbf{X}\mathbf{X}^\top)^{-1}\mathbf{y}$, which is the Moore-Penrose pseudoinverse solution and well-known as the minimum l_2 norm solution to eq. (7).

Although the discussion has considered the very simple problem of linear regression, we will see throughout this tutorial that many of these themes have parallels when training deep neural networks. Specifically, in Section 3.1 we detail how the dynamics of gradient descent are restricted to a low-rank subspace at every iteration when training deep, linear neural networks; that structure is leveraged in Section section 3.2 and Section 3.3 to reduce computational requirements for fine-tuning and training deep networks. In Section 4.2 we discuss how adding l_2 regularization on the parameters of multi-layer models is often equivalent to adding low-rank regularization on the model predictions, then we describe settings where model training implicitly adds l_2 regularization (and hence promotes low-rank structure) through either the implicit bias of gradient descent (Section 4.3) or via heuristics used to train deep networks which stochastically mask the data or latent representations of the data such as Masked Autoencoders or Dropout (Section 4.4).

3 Low-Rank Structure at Every Iteration of Gradient Dynamics

3.1 Analysis of Training Dynamics

In this section, we look at how low-dimensional structure emerges in the training dynamics of deep linear networks. Many works study deep linear networks due to being much easier to analyze compared to their nonlinear counterparts, while still maintaining a notion of intermediate feature representations. Such works are able to demonstrate a particular implicit bias towards low-rank structure in the network weights, yielding insight into the geometry of feature representations, yet often only identify low-rank structure at the end of optimization. Instead, the result we present here discusses low-rank structure *throughout* the learning process, making it amenable to exploitation by a structure-aware optimization algorithm. To illustrate this concept, we consider a simplified deep matrix factorization setting. Specifically, we train a fully connected deep linear network, as formulated in eq. (3), without nonlinear activations or biases. Additionally, we assume that the input \mathbf{X} is either the identity matrix or whitened data, as described in eq. (6). Specifically, we consider

$$\min_{\Theta} \frac{1}{2} \underbrace{\|\mathbf{W}_L \cdots \mathbf{W}_1 - \Phi\|_F^2}_{\mathcal{L}(\Theta)} + \frac{\lambda}{2} \sum_{l=1}^L \|\mathbf{W}_l\|_F^2, \quad (11)$$

where $\Phi \in \mathbb{R}^{d \times d}$ is the target matrix, which can be taken as $\Phi = \mathbf{Y}\mathbf{X}^\top(\mathbf{X}\mathbf{X}^\top)^{-1}$ as in eq. (6) with $k = d$, and $\Theta = \{\mathbf{W}_l\}_{l=1}^L$ are the network parameters with $\mathbf{W}_l \in \mathbb{R}^{d \times d}$ for each $l \in [L]$. For each weight matrix \mathbf{W}_l , the gradient descent updates can be written as follows:

$$\mathbf{W}_l^{(t+1)} = (1 - \eta\lambda)\mathbf{W}_l^{(t)} - \eta\nabla_{\mathbf{W}_l} \mathcal{L}(\Theta^{(t)}), \quad \forall t = 0, 1, 2, \dots, \quad (12)$$

where $\eta > 0$ is the learning rate. When we have $\lambda > 0$, this is called weight decay due to the down-weighting of the weights from the previous iteration.

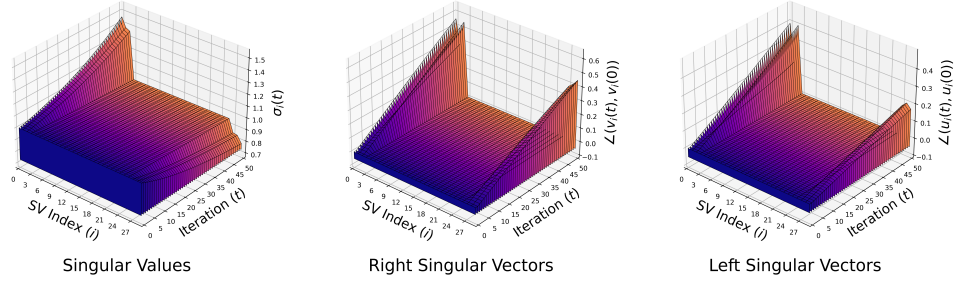


Figure 3: Evolution of SVD of weight matrices for deep matrix factorization. We visualize the SVD dynamics of the first layer weight matrix of an $L = 3$ layer deep matrix factorization for a random matrix with $d = 30$, $r = 3$, $\epsilon_l = 1$ throughout GD without weight decay ($\lambda = 0$). *Left:* Magnitude of the i -th singular value $\sigma_i(t)$ at iteration t . *Middle:* Angle $\angle(\mathbf{v}_i(t), \mathbf{v}_i(0))$ between the i -th right singular vector at iteration t and initialization. *Right:* Angle $\angle(\mathbf{u}_i(t), \mathbf{u}_i(0))$ between the i -th left singular vector at iteration t and initialization.

We now present the main result from [8], which demonstrates that the implicit bias of gradient descent in minimizing eq. (11) with low-rank data arises because the entire trajectory of weight updates remains confined to a specific low-dimensional subspace. To show this, we make the following assumptions:

A1. Φ is a rank r matrix with $r \ll d$ (i.e., low-rank);

A2. Each initial weight matrix $\mathbf{W}_l^{(0)}$ is an ϵ_l -scaled orthogonal matrix for some $\epsilon_l > 0$, i.e.,

$$\mathbf{W}_l^{(0)} \mathbf{W}_l^{(0)\top} = \mathbf{W}_l^{(0)\top} \mathbf{W}_l^{(0)} = \epsilon_l^2 \mathbf{I}_d.$$

Based on this, the following result states that the gradient updates only occur in $2r$ -dimensional subspaces of the left and right singular spaces of each weight matrix \mathbf{W}_l .

Theorem 2. Suppose we perform gradient descent on eq. (11) with the iterates given in eq. (12). Under assumptions A1 and A2, the SVD of weight matrix $\mathbf{W}_l^{(t)} \in \mathbb{R}^d$ can be decomposed as

$$\mathbf{W}_l^{(t)} = \begin{bmatrix} \mathbf{U}_{l,1}^{(t)} & \mathbf{U}_{l,2} \end{bmatrix} \begin{bmatrix} \Sigma_l^{(t)} & \mathbf{0}_{2r \times (d-2r)} \\ \mathbf{0}_{(d-2r) \times 2r} & \rho_l^{(t)} \mathbf{I}_{(d-2r)} \end{bmatrix} \begin{bmatrix} \mathbf{V}_{l,1}^{(t)} & \mathbf{V}_{l,2} \end{bmatrix}^\top \quad \forall l \in [L], \quad \forall t = 0, 1, 2, \dots,$$

where $\Sigma_l^{(t)} \in \mathbb{R}^{2r \times 2r}$ is diagonal with $\Sigma_l^{(0)} = \epsilon_l \mathbf{I}_{2r}$, $d - 2r$ singular values are identical with

$$\rho_l^{(t)} = \rho_l^{(t-1)} (1 - \eta\lambda - \eta \prod_{k \neq l} \rho_k^{(t-1)^2}) \approx \epsilon_l (1 - \eta\lambda)^t \quad (13)$$

where the orthonormal matrices $(\mathbf{U}_{l,2})_{l=1}^L, (\mathbf{V}_{l,2})_{l=1}^L \subset \mathcal{O}^{d \times (d-2r)}$ are independent of t and satisfy $\mathbf{V}_{l+1,2} = \mathbf{U}_{l,2}$ for all $l \in [L - 1]$, and the approximation in eq. (13) uses $\rho_l^{(0)} = \epsilon_l$ and is more accurate as L increases.

This theorem characterizes the decomposition of weight matrices at each iteration of gradient descent. Although it applies to a simplified setting—a deep linear network trained with l_2 loss—it provides valuable insights into the low-rank structures throughout the learning dynamics of deep networks. The decomposition in the theorem, in the absence of weight decay ($\lambda = 0$), is visualized in Figure 3, where only $2r$ singular values and vectors evolve during gradient descent. This suggests that when ϵ_l is sufficiently small, the depth L is large enough, and/or weight decay is applied ($\lambda > 0$), a significant portion of singular values decay to zero as $t \rightarrow \infty$.

To understand why this structured decomposition emerges, let us build some intuition for the case of $L = 2$. The key is that we identify the $(d - 2r)$ -dimensional subspace where gradient updates *do not* occur.

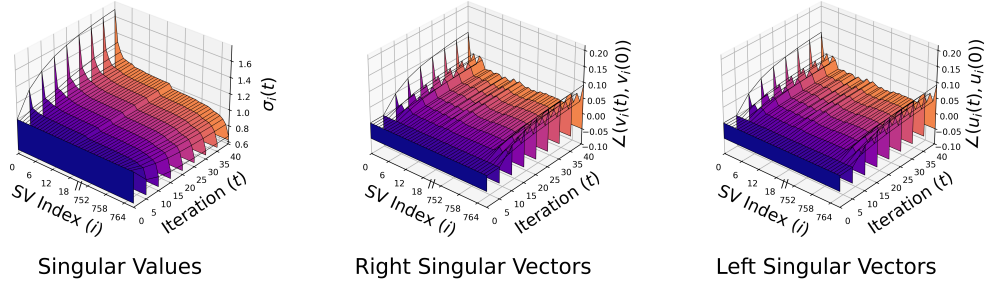


Figure 4: Evolution of SVD of weight matrices for deep low-rank adaptation. We visualize the SVD dynamics of an $L = 3$ layer deep matrix factorization’s end-to-end product employed for fine-tuning the 11th layer value matrix in BERT, with $d = 768$, $\epsilon_t = 1$ throughout Adam. *Left:* Magnitude of the i -th singular value $\sigma_i(t)$ at iteration t . *Middle:* Angle $\angle(\mathbf{v}_i(t), \mathbf{v}_i(0))$ between the i -th right singular vector at iteration t and initialization. *Right:* Angle $\angle(\mathbf{u}_i(t), \mathbf{u}_i(0))$ between the i -th left singular vector at iteration t and initialization.

Note we will now repeatedly rely on the properties of our initialization, that weight matrices are orthogonal and scaled by ϵ_t . The gradient with respect to $\mathbf{W}_1^{(0)}$ and $\mathbf{W}_2^{(0)}$ is thus given by

$$\begin{aligned}\nabla_{\mathbf{W}_1} \mathcal{L}(\Theta^{(0)}) &= \mathbf{W}_2^{(0)\top} (\mathbf{W}_2^{(0)} \mathbf{W}_1^{(0)} - \Phi) = \epsilon_2^2 \mathbf{W}_1^{(0)} - \mathbf{W}_2^{(0)\top} \Phi, \text{ and} \\ \nabla_{\mathbf{W}_2} \mathcal{L}(\Theta^{(0)}) &= (\mathbf{W}_2^{(0)} \mathbf{W}_1^{(0)} - \Phi) \mathbf{W}_1^{(0)\top} = \epsilon_1^2 \mathbf{W}_2^{(0)} - \Phi \mathbf{W}_1^{(0)\top}.\end{aligned}$$

From here, we can construct $(d - 2r)$ -dimensional left and right subspaces \mathcal{U}_1 and \mathcal{V}_1 of $\mathbf{W}_1^{(0)}$ that lie in the left and right nullspaces of $\nabla_{\mathbf{W}_1} \mathcal{L}(\Theta^{(0)})$ respectively. Specifically, let $\mathcal{V}_1 = \mathcal{N}(\Phi) \cap \mathcal{N}(\Phi^\top \mathbf{W}_2^{(0)} \mathbf{W}_1^{(0)})$, where \mathcal{N} denotes nullspace, and let $\mathcal{U}_1 = \text{span}(\{\mathbf{W}_1^{(0)} \mathbf{v}, \forall \mathbf{v} \in \mathcal{V}_1\})$, which we will denote with shorthand $\mathcal{U}_1 = \{\mathbf{W}_1^{(0)} \mathcal{V}_1\}$. As a result, $\dim(\mathcal{U}_1) = \dim(\mathcal{V}_1) \geq d - 2r$.

This proper choice of subspaces directly results in the decomposition of Theorem 2. The way we defined it, there are at least $d - 2r$ pairs of vectors $(\mathbf{u}, \mathbf{v}) \in \mathcal{U}_1 \times \mathcal{V}_1$ with $\mathbf{W}_1^{(0)} \mathbf{v} = \epsilon_1 \mathbf{u}$, while $\nabla_{\mathbf{W}_1} \mathcal{L}(\Theta^{(0)}) \mathbf{v} = \epsilon_2^2 \epsilon_1 \mathbf{u}$ and

$$\nabla_{\mathbf{W}_1} \mathcal{L}(\Theta^{(0)})^\top \mathbf{u} = \epsilon_2^2 \mathbf{W}_1^{(0)\top} \mathbf{u} - \Phi^\top \mathbf{W}_2^{(0)} \mathbf{u} = \epsilon_2^2 \epsilon_1 \mathbf{v} - \Phi^\top \mathbf{W}_2^{(0)} (\epsilon_1 \mathbf{W}_1^{(0)} \mathbf{v}) = \epsilon_2^2 \epsilon_1 \mathbf{v}$$

by using the second intersected null space in the definition of \mathcal{V}_1 . Therefore, eq. (12) gives us:

$$\begin{aligned}\mathbf{W}_1^{(1)} \mathbf{v} &= \left((1 - \eta\lambda) \mathbf{W}_1^{(0)} - \eta \nabla_{\mathbf{W}_1} \mathcal{L}(\Theta^{(0)}) \right) \mathbf{v} = \epsilon_1 (1 - \eta\lambda - \eta\epsilon_2^2) \mathbf{u}, \\ \mathbf{W}_1^{(1)\top} \mathbf{u} &= \left((1 - \eta\lambda) \mathbf{W}_1^{(0)\top} - \eta \nabla_{\mathbf{W}_1} \mathcal{L}(\Theta^{(0)})^\top \right) \mathbf{u} = \epsilon_1 (1 - \eta\lambda - \eta\epsilon_2^2) \mathbf{v},\end{aligned}$$

meaning that $(\mathbf{u}, \mathbf{v}) \in \mathcal{U}_1 \times \mathcal{V}_1$ remain singular vectors after the gradient step, but their singular value shrinks by a factor of $1 - \eta\lambda - \epsilon^2$ (independent of Φ). Similar invariant subspaces emerge in the second layer – in fact, the invariant subspaces align across the two layers. Taking $\mathcal{V}_2 = \mathcal{U}_1$, so that

$$\{\mathbf{W}_1^{(0)\top} \mathcal{V}_2\} = \{\mathbf{W}_1^{(0)\top} \mathcal{U}_1\} = \mathcal{V}_1 \subset \mathcal{N}(\Phi)$$

by construction of \mathcal{V}_1 , we have that any $\mathbf{v} \in \mathcal{V}_2$ satisfies $\nabla_{\mathbf{W}_2} \mathcal{L}(\Theta^{(0)}) \mathbf{v} = \epsilon_1^2 \mathbf{W}_2^{(0)} \mathbf{v} = \epsilon_1^2 \epsilon_2 \mathbf{u}$ defining \mathcal{U}_2 in the analogous way to the first step. While this argument is for $L = 2$, the result can be generalized to arbitrary L , as can be seen in the supplementary material of [8]. We emphasize once again that we define the subspaces where training does not occur and subsequently determine the invariant training subspaces as their orthogonal complements.

We highlight the key ingredients for the emergence of low-rank structure in the optimization of deep matrix factorizations. First, we require that the target data Φ is low rank – when $\Phi = \mathbf{Y} \mathbf{X}^\top (\mathbf{X} \mathbf{X}^\top)^{-1}$, this is satisfied due to the columns of \mathbf{Y} often lying in a much lower dimensional subspace compared to the input

dimensionality/network width d , and one can show a similar result to Theorem 2 when Y has $k \ll d$ rows – see Appendix C in the supplementary materials for more details. The second assumption we make is that the weight matrices are initialized to be scaled orthogonal matrices – this is approximately satisfied when (1) the entries of $\mathbf{W}_l^{(0)}$ are drawn *iid* from a Gaussian distribution, which is utilized in practice, and (2) d is large, corresponding to the wide and overparameterized nature of modern deep networks. To ensure that the final weights are low-rank, we require some form of regularization, whether that be implicit via small-scale initialization or explicit via weight-decay. Finally, we have assumed that the objective is of the form (11), where we employ the squared error loss with respect to some target. In Section 3.2, we will see how matrix factorizations are employed to efficiently fine-tune large language models, where the training objective is significantly more complicated. Yet even in this setting, similar phenomena in the SVD dynamics of the weights emerge, as shown in Figure 4 (compare with Figure 3). Later, we will see how this can be exploited for efficient and robust fine-tuning.

Several works laid the foundation for analyzing the dynamics of gradient descent for deep linear networks, along with its connection to implicit low-rank bias in gradient descent for low-rank factorization. [9] pioneered this analysis, deriving closed-form solutions for singular values under gradient flow in a special initialization setting where weight singular vectors remain stationary. [10] extended this to general initializations, establishing a stronger link between singular vector stationarity and gradient alignment. More recently, [8] leveraged low-rank gradients to construct orthogonal singular subspaces, distinguishing between learning-relevant and stationary components. Unlike prior work, it considers discrete-time gradient descent, arbitrary orthogonal initialization, and the role of low-rank training in compressing overparameterized deep matrix factorization. In a related but distinct direction, [11] analyzed the alignment of deep network weights in cases where they converge to a rank-one matrix. Additionally, [12] introduced a different perspective on low-rankness in training dynamics through greedy low-rank learning, where gradient descent incrementally fits the best rank-one approximation to the residual error. Beyond these works, a broader literature explores the implicit low-rank bias of gradient descent, though not necessarily focusing on the low-dimensional structure of training dynamics—this will be discussed further in Section 4.

3.2 Low-Rank Adaptation for Fine-tuning Large-Scale Models

Thus far, we have illustrated how low-rank structure emerges implicitly in the learning dynamics of the simple deep linear model. In this section, we discuss how this insight has been explicitly leveraged for parameter efficient fine-tuning of large-scale pre-trained models. Fine-tuning, or adaptation, is the process of updating all or a subset of a pre-trained model’s parameters to adapt it to a downstream task. Concretely, let $\overline{\mathbf{W}}_l \in \mathbb{R}^{d \times d}$ denote a pre-trained weight matrix for a particular layer l , and let us introduce a trainable weight matrix $\Delta \mathbf{W}_l \in \mathbb{R}^{d \times d}$. During inference, we consider the effective weight \mathbf{W}_l :

$$\mathbf{W}_l = \overline{\mathbf{W}}_l + \Delta \mathbf{W}_l, \quad (14)$$

where $\Delta \mathbf{W}_l$ is the trained (or adapted) weight matrix and $\overline{\mathbf{W}}_l$ remains fixed (or frozen) throughout the entire process. However, optimizing $\Delta \mathbf{W}_l$ for each dense layer of the pre-trained model can be as computationally expensive as training from scratch. To deal with the challenge, Low-Rank Adaptation (LoRA) [2] reduces computational burden by assuming that overparameterized models reside in low-dimensional intrinsic subspaces. Specifically, it assumes that the change in weights $\Delta \mathbf{W}_l$ also has low intrinsic rank, and considers the following effective weight instead:

$$\mathbf{W}_l = \overline{\mathbf{W}}_l + \mathbf{B}_l \mathbf{A}_l, \quad (15)$$

where $\mathbf{B}_l \in \mathbb{R}^{d \times r}$ and $\mathbf{A}_l \in \mathbb{R}^{r \times d}$ with $r \ll d$ are the trainable weights constrained to have at most rank r . This essentially considers a low-rank factorization of $\Delta \mathbf{W}_l$, such that as opposed to fine tuning *all* entries of $\Delta \mathbf{W}_l$ (which amounts to a dimension d^2 search space), the parameterization (15) restricts the number of learnable parameters to $2dr$, allowing us to significantly reduce memory and computation requirements if $r \ll d$. For simplicity, we discuss based upon square weight matrices here, but in practice this can be extended to any size weight matrix as long as each dimension is greater than r . In this section, we focus on two key aspects of LoRA which has been heavily investigated recently: how to effectively choose two key hyperparameters, the learning rate and the rank.

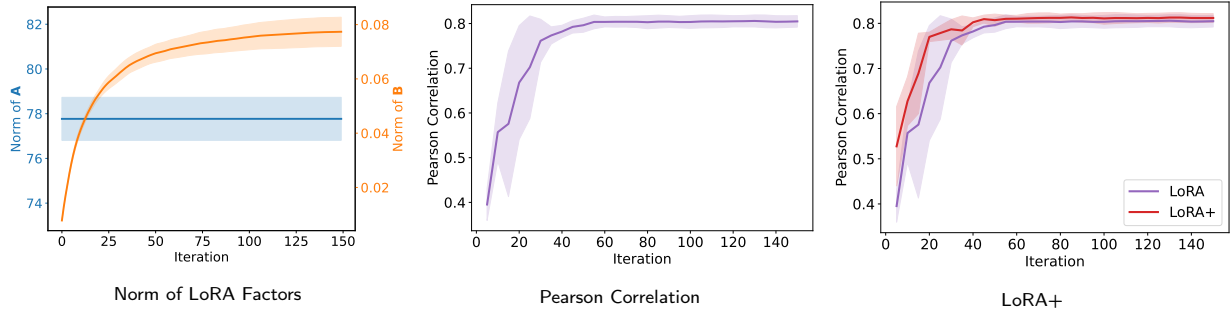


Figure 5: Highlighting the inefficiency of LoRA that arises from using asymmetric initializations on BERT. Existing papers explore ways to balance learning between the two LoRA factors and justify whether one initialization is preferable to another. The norm of the two factors over training iterations. Middle: The Pearson correlation over training iterations. Note that even though the norm of \mathbf{A} remains nearly constant throughout training, the test performance, as measured by the Pearson correlation, still indicates good accuracy. Right: By using discrepant learning rates as in LoRA+ [13], we obtain faster convergence.

3.2.1 Choosing the Learning Rate

Generally, given some learning rate $\eta > 0$, we update the LoRA parameters using some gradient-based method:

$$\mathbf{B}_l^{(t+1)} = \mathbf{B}_l^{(t)} - \eta \cdot \nabla_{\mathbf{B}_l} \mathcal{L}(\Theta), \quad \mathbf{A}_l^{(t+1)} = \mathbf{A}_l^{(t)} - \eta \cdot \nabla_{\mathbf{A}_l} \mathcal{L}(\Theta), \quad (16)$$

where $\mathcal{L}(\cdot)$ denotes the loss function and Θ represents the collection of network parameters. For initialization (at $t = 0$), we set one of the factors to the zero matrix so that fine-tuning begins from the pre-trained model. Concretely, let $\mathbf{a}_{l,i} \in \mathbb{R}^d$ denote a column of \mathbf{A}_l and let $\mathbf{b}_{l,i}^\top \in \mathbb{R}^d$ denote a row of \mathbf{B}_l . For all $i \in [r]$, the factors are typically initialized as follows [2]:

$$\mathbf{b}_{l,i}^{(0)\top} = \mathbf{0}_d \quad \text{and} \quad \mathbf{a}_{l,i}^{(0)} \sim \mathcal{N}(\mathbf{0}, \sigma^2 \mathbf{I}_d), \quad \text{where} \quad \sigma^2 = \Theta(d^{-1}). \quad (17)$$

While we use a Gaussian distribution for the initialization above, it is important to note that any other distribution with finite variance can be used. The variance of the factor is chosen to prevent any possible numerical instabilities.

While this initialization was designed to enable fine-tuning from the pre-trained model, Hayou et al. [13] found that the asymmetry in the factors leads to “inefficient feature learning”. They define efficient feature learning as a setup in which the norm of the change in the LoRA updates remains constant at $\Theta(1)$. However, the asymmetry causes the norm of one factor to change much faster than the other, leading to inefficiencies (i.e., slower convergence). We illustrate this point on the lefthand side of Figure 5, where we fine-tune a BERT model on the STS-B dataset using a learning rate of $\eta = 10^{-4}$ and rank $r = 8$. Despite the test loss increasing, measured in terms of the Pearson correlation, the norm of one factor hardly changes throughout training, while the norm of the other factor changes rapidly. To account for these observations, Hayou et al. [13] propose an algorithm called LoRA+ using discrepant learning rates. That is, rather than using the same learning rate for both factors as in Equation (16), we use discrepant learning rates as follows:

$$\mathbf{B}_l^{(t+1)} = \mathbf{B}_l^{(t)} - \gamma\eta \cdot \nabla_{\mathbf{B}_l} \mathcal{L}(\Theta), \quad \mathbf{A}_l^{(t+1)} = \mathbf{A}_l^{(t)} - \eta \cdot \nabla_{\mathbf{A}_l} \mathcal{L}(\Theta),$$

for some constant $\gamma > 0$. This is the main idea behind LoRA+, where they claim that we should use a larger learning rate for \mathbf{B}_l such that we can account for the differences in the norms. On the righthand side of Figure 5, we observe that we can indeed obtain faster convergence with LoRA+ using $\lambda = 2$ in the same BERT model setup. The work LoRA-Done-RITE [14] builds upon this observation to propose an adaptive preconditioned learning rate that balances the factors. Both algorithms have been shown to improve convergence speed and achieve superior performance over the vanilla LoRA method, and we can expect future research to further address these inefficiencies and develop more efficient LoRA adapters.

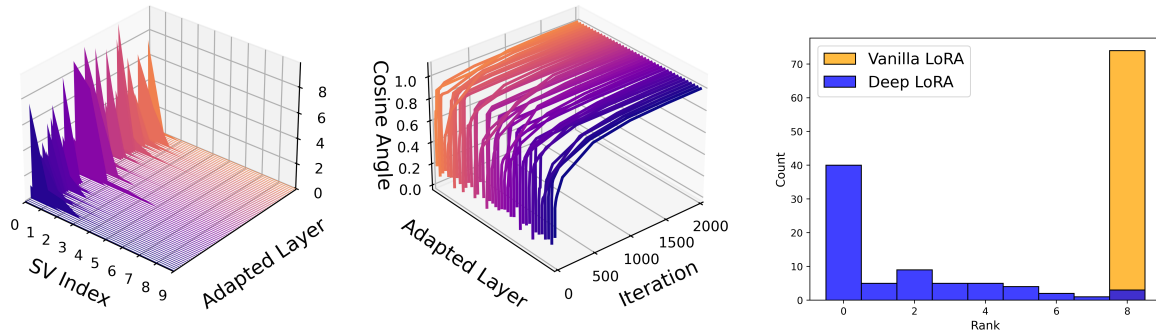


Figure 6: Invariant low-dimensional subspaces in deep overparameterized adaptation of language models. Fine-tuning BERT [17] with deep overparameterized adaptation on the STS-B dataset [18] *Left: Singular value* spectra across all adapted layers at the end of fine-tuning. *Middle: Alignment of subspaces* formed by top 8 right singular vectors between current adapted weights and final adapted weights throughout training. *Right: Deep LoRA finds lower ranked adapters* as opposed to LoRA, allowing it to have better test loss in the sample-starved regime.

3.2.2 Choosing the Rank Allocation

A separate line of work focuses on efficient methods for selecting the other hyperparameter in LoRA: the rank. The choice of rank presents a tradeoff – if the rank is too small, the number of parameters in the LoRA adapters may be insufficient to capture all necessary information of the downstream data. Conversely, if the rank is too large, it will overfit and can slow down both training and inference. Moreover, it is widely believed that certain layers require less updating than others. Shallow layers near the input typically extract generic features useful across multiple tasks, making extensive fine-tuning unnecessary. Consequently, allocating a large rank to these layers may be inefficient. However, selecting an optimal rank for each of the L layers via cross-validation would demand substantial computational resources, potentially negating the efficiency gains of LoRA. To address this challenge, several methods have been proposed. We will discuss two distinct approaches: AdaLoRA [15] and Deep LoRA [8], both of which enable flexible rank allocation for weight updates at each layer.

The development of AdaLoRA [15] approaches this problem by allocating a rank budget to the overall system. The goal is to then find the allocation of this budget across layers during the fine-tuning process itself. Their approach is to start with some budget schedule, $\mathbf{b}^{(t)}$, that they will enforce at training pass t . This schedule should start with some maximum rank at each layer and end at the desired total budget. So if we want the maximum rank to be \bar{r} for L weight matrices, then $\mathbf{b}^{(0)} = \bar{r}L$, and if we can accommodate a total budget equivalent to rank- r updates for each of L weight matrices, we have $\mathbf{b}^{(t)} \rightarrow rL$. Then in each pass, we update the LoRA adapter not in pairs $\mathbf{B}_l\mathbf{A}_l$, but in triplets $\mathbf{P}_l\mathbf{\Lambda}_l\mathbf{Q}_l$, where $\mathbf{\Lambda}_l$ is a diagonal matrix whose entries can be set to zero in order to decrease the rank budget allocated at this layer. They choose which entries of $\{\mathbf{\Lambda}_l\}_{l=1}^L$ to set to zero by scoring them across all layers in each fine-tuning epoch. Several possible scoring functions are studied in the paper. In order for the zeroing of an entry to be more meaningful in the decomposition $\mathbf{P}_l\mathbf{\Lambda}_l\mathbf{Q}_l$, they also ideally would have $\mathbf{P}_l, \mathbf{Q}_l$ be orthogonal matrices, as in Theorem 1. To approximate this condition, they use soft enforcement by regularization with $\|\mathbf{P}\mathbf{P}^\top - \mathbf{I}\| + \|\mathbf{Q}\mathbf{Q}^\top - \mathbf{I}\|$ in the objective function. While these additions create some overhead, the experiments in [16] show improved accuracy as compared to a fixed rank allocation when fine-tuning on several benchmark datasets.

Deep LoRA [8] takes the approach of using overparameterization to implicitly allocate a rank budget by inducing a low-rank structure that can vary in rank across layers. The theory in Section 3.1 for deep matrix factorization provides the starting point for Deep LoRA. Roughly speaking, recall that in the deep matrix factorization setting, the residual singular values are suppressed by a factor of a power of L , where L is the depth. In fact, recent literature on overparameterization shows that the deeper linear factorizations are generally biased toward lower rank solutions [10]. We show evidence of the low-rank bias in Figure 6, where a deep nonlinear network has been fine-tuned with an overparameterized version of LoRA, where we have

three factors each of size $d \times d$. From the figure, we can see that (i) all the converged weights $\{\Delta \mathbf{W}_l\}_{l=1}^m$ are very low-rank (left panel), (ii) the learning dynamics each for each weight *approximately* stay within the same invariant subspace throughout the iterations (middle panel).

Of course, it would be inefficient to adapt with full $d \times d$ factors, as that would be as computationally burdensome as full fine-tuning. However, these empirical observations suggest that deep, overparameterized factorizations for fine-tuning are highly compressible. Thus, we can apply a compression method to (i) leverage the benefits of depth in overparameterization for LoRA and (ii) mitigate the overhead of added depth by reducing the width of the intermediate layers. This is the idea of Deep LoRA. Each weight matrix is updated with

$$\mathbf{W}_l = \overline{\mathbf{W}}_l + \underbrace{\mathbf{C}_l \mathbf{B}_l \mathbf{A}_l}_{=: \Delta \mathbf{W}_l},$$

where $\mathbf{A}_l \in \mathbb{R}^{r \times d}$, $\mathbf{B}_l \in \mathbb{R}^{r \times r}$, and $\mathbf{C}_l \in \mathbb{R}^{d \times r}$, ideally capturing the training subspace for a deep linear network discussed in Theorem 2. However, the major difference in Deep LoRA from the matrix factorization setting in Section 3.1 is that the target is not exactly low-rank and so the updates are not expected to occur within a fixed, invariant subspace across the training iterations. To this end, similar to the approach in LoRA+, Deep LoRA employs a discrepant learning rate that allows the outer factors $\mathbf{C}_l, \mathbf{A}_l$ to change, but more slowly than the inner factor \mathbf{B}_l . For some $\gamma > 0$, we have:

$$\mathbf{C}_l^{(t+1)} = \mathbf{C}_l^{(t)} - \gamma \eta \cdot \nabla_{\mathbf{C}_l} \mathcal{L}(\Theta), \mathbf{B}_l^{(t+1)} = \mathbf{B}_l^{(t)} - \eta \cdot \nabla_{\mathbf{B}_l} \mathcal{L}(\Theta), \mathbf{A}_l^{(t+1)} = \mathbf{A}_l^{(t)} - \gamma \eta \cdot \nabla_{\mathbf{A}_l} \mathcal{L}(\Theta).$$

Following the setup of the previous section, we fine-tune a BERT model using Deep LoRA with a rank of $r = 8$ and depth $L = 3$. In Figure 6 (right panel), we show that Deep LoRA indeed implicitly finds adapters with varying ranks. In particular, the solutions found have lower effective rank than those obtained using vanilla LoRA (i.e., $L = 2$), which helps explain why Deep LoRA achieves better test accuracy in the regime of limited fine-tuning samples [8].

3.3 Low-Rank Training

More recently, the implicit low-rank structures in learning dynamics [8] (Section 3.1), coupled with the success of LoRA (Section 3.2), have inspired researchers to explicitly explore low-rank structures for training large-scale deep networks. Instead of introducing additional low-rank adapters and hence not altering the training dynamics [19, 20, 21], these approaches have the potential to significantly reduce the computational and memory requirements of training large-scale neural networks by approximating the gradient updates of weight matrices with low-rank factorizations.

However, the optimal weights of nonlinear neural networks are often *not* inherently low-rank, as evidenced by the fact that LoRA may not always match the performance of full-rank fine-tuning and often benefits from an initial full-rank training phase to effectively leverage the low-rank subspace [2]. Nonetheless, several recent works [8, 20, 21, 22] showed that gradient updates of the weights are approximately low-rank, where the gradients approximately reside in slowly changing low-rank subspace across the learning dynamics. For deep linear models, the low-rank structure of gradient updates follows directly from our training dynamics analysis in Section 3.1 and the findings in [8, 1], where the gradient captures the difference between two consecutive weight updates within the same low-rank subspace. More recent work [20] justifies the low-rank gradient for reversible nonlinear networks, showing the gradient becomes low-rank during training when it follows certain parametric forms.

Specifically, if we consider the weight matrix of any given layer (e.g., l th layer) in a neural network, then slow changing low-rank gradient implies that we can approximate the weight \mathbf{W}_{KT} at the KT -th iteration

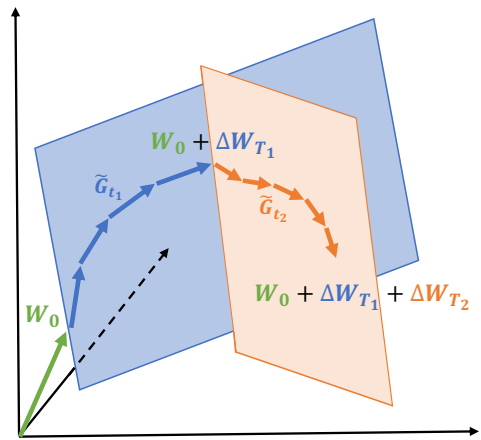


Figure 7: An illustration of learning through low-rank subspaces using GaLore.

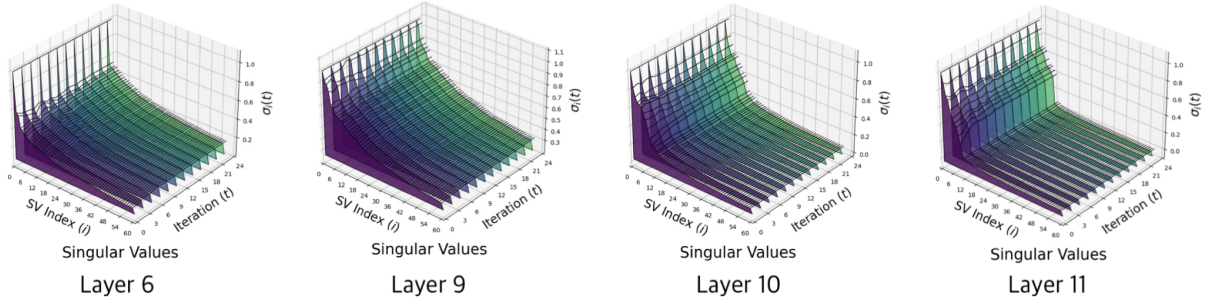


Figure 8: Singular values across layers of the ViT of the FC2 weight matrix. While the singular values of the shallower layers do not clearly exhibit a low-rank structure, the deeper layers certainly do.

by

$$\mathbf{W}_{KT} = \mathbf{W}_0 + \sum_{k=1}^K \Delta \mathbf{W}_{T_k}, \text{ where } \Delta \mathbf{W}_{T_k} = \sum_{t_k=1}^T \mathbf{G}_{t_k}, \quad (18)$$

where \mathbf{W}_0 is the weight initialization, T denotes the window size of each subspace, and \mathbf{G}_{t_k} denotes the t -th gradient update in the k -th subspace \mathbf{U}_k . In other words, the accumulated gradient $\Delta \mathbf{W}_{T_k}$ lies within a low-dimensional subspace \mathbf{U}_k , where the subspace \mathbf{U}_k dynamically changes with respect to k [19, 20], see Figure 7 for an illustration. This phenomenon can yield significant benefits: by restricting updates to a subspace of reduced dimension, one can potentially reduce both computational cost and memory usage, since operations in higher-rank dimensions become negligible [19, 20].

Exploring Low-rank Gradient for Low-Rank Training In practice, many recent works leverage low-rank structures in the gradient to reduce memory usage. Specifically, based upon (18), Gradient Low-Rank Projection (GaLore) method [20] that leverages the gradient low-rank structures in (18) through subspace projection

$$\tilde{\mathbf{G}}_{t_k} = \mathbf{P}_k \rho(\mathbf{P}_k \mathbf{G}_{t_k} \mathbf{Q}_k^\top) \mathbf{Q}_k^\top, \quad (19)$$

to better capture the information of the full-rank gradient \mathbf{G}_{t_k} . Here, $\mathbf{P}_k \in \mathbb{R}^{m \times r}$ and $\mathbf{Q}_k \in \mathbb{R}^{n \times r}$ are the subspace projection matrices of the original gradient $\mathbf{G}_{t_k} \in \mathbb{R}^{m \times n}$, and $\rho(\cdot)$ is an operator on gradient that flexibly encompasses a variety of gradient-based methods such as momentum or Adam. To compensate for the dynamically changing subspaces, GaLore updates \mathbf{P}_k periodically by computing the full SVD of $\mathbf{G}_{t_k=1}$ at the beginning of every T epoch. We present the algorithm applying GaLore to Adam in Algorithm 1 in the appendices, where $\rho(\cdot)$ is instantiated as the Adam update rule. As shown in [20], GaLore significantly improved memory efficiency when training LLMs, reducing optimizer state memory usage by up to 65.5%. Inspired by (18), there has also been another ReLoRA method [19] that uses randomly initialized LoRA pairs $\mathbf{B}_k \mathbf{A}_k$ to approximate $\Delta \mathbf{W}_{T_k}$ and merge them with the full weights \mathbf{W}_0 every T iterations. Compared to ReLoRA, GaLore achieves better performance with similar memory cost, but at the cost of extra computation time due to extra projection operators and computing the initial full rank gradient $\mathbf{G}_{t_k=1}$ for each $k = 1, \dots, K$. Moreover, when ReLoRA uses the full-rank gradient as initializations, it can be shown that it is equivalent to GaLore; more detailed proof is shown in Appendix D.

Improving Low-Rank Training via Adaptive Rank Allocation across Different Layers and Components

While GaLore offers remarkable improvements in memory efficiency, its uniform treatment of different layers and usage of the same training window can be suboptimal for large-scale deep learning models. This phenomenon is illustrated in Figure 8, which shows the singular values of different MLP layers in ViT models throughout training. As observed, deeper layers tend to exhibit more pronounced low-rank structure

compared to shallower layers. A similar trend is evident in the value weight matrices of the self-attention components; see Appendix D for details.

Therefore, the follow-up results, such as Weight Low-Rank Projection (WeLore) [21], reveal the significant differences in effective ranks across different layers and training epochs in LLMs. AdaRankGrad [22] demonstrates that layer gradient ranks gradually decrease as training converges, asymptotically approaching one. Leveraging this, it adaptively reduces gradient rank during Adam optimization using an efficient online low-rank projection update. The method dynamically adjusts each layer’s projection dimension based on training progress, exploiting the gradual reduction in gradient dimensionality to perform updates in a lower-dimensional space, thereby reducing memory usage. Projection matrices are updated based on a convergence criterion, ensuring timely adjustments and preventing premature or delayed subspace transitions, leading to faster convergence. Compared to GaLore, AdaRankGrad further improves memory efficiency for pretraining of LLMs [22].

Moreover, different components of Transformer models exhibit distinct low-rank structures that can be leveraged for compression. For instance, the recent DeepSeek V3 model [3] achieves significant memory savings during training by only factorizing the query matrix into a low-rank form within the multi-head attention mechanism, all while maintaining strong performance. Finally, in a broader perspective, the low-rank structure is one example of a more general class of compressive structures that have gained recent attention. We refer interested readers to in the appendices for a more detailed discussion.

4 Low-Rank Structure at the Convergence of Gradient Methods

4.1 Implicit Regularization

As we have seen above, low-rank structure can arise due to the dynamics of a particular optimization algorithm that enforces (or exploits in the case of LoRA methods) the low-rank structure throughout the optimization process (i.e., at every iteration of the optimization algorithm the low-rank structure is present). However, low-rank structure also arises through other means in a variety of deep learning settings. In particular, in this section we explore various conditions and algorithms where the final solution the algorithm converges to has low-rank structure. If we recall the simple example of overparameterized linear regression from 2.3, we observed that if we initialized the parameters at the origin ($w^{(0)} = 0$), then of the infinitely many possible choices of parameters that perfectly fit the data, gradient descent would implicitly find the parameters that fit the data with the minimum l_2 norm,

$$\underbrace{\min_w \frac{1}{2} \|\mathbf{y} - \mathbf{X}\mathbf{w}\|_F^2}_{\text{Original Overparameterized Problem}} \xrightarrow{\text{Gradient Descent}} \underbrace{\min_w \|\mathbf{w}\|_2 \text{ s.t. } \mathbf{y} = \mathbf{X}\mathbf{w}}_{\text{Problem Implicitly Solved by Gradient Descent}} \quad (20)$$

As a result, l_2 regularization has been implicitly added to the problem due to the dynamics of gradient descent, and below, we will see a variety of additional settings where l_2 regularization also gets implicitly added as part of the network training process. At first, this does not present an immediate link to low-rank structure, but as we discuss in the next section, in many models consisting of sequential application of linear operators, applying l_2 regularization to the model parameters is equivalent to adding low-rank regularization to the overall prediction of the model.

4.2 Low-Rank from l_2 Regularization

A key link that arises in the emergence of low-rank structure is the general idea that in many settings adding l_2 regularization on the weight parameters can result in adding low-rank inducing regularization on the predictions of the model on the training set. In particular, recall the deep matrix factorization objective (11) in Section 3.1, where we have observed that optimizing this objective with gradient descent will result in low-rank parameter matrices when l_2 regularization is used (i.e., $\lambda > 0$), commonly referred to as *weight decay* in the context of deep learning, and a natural question is whether this behavior as a idiosyncratic to the gradient descent dynamics or a more general phenomenon. As we will see below, low-rank solutions are, in fact, promoted by the use of l_2 regularization on the model weights due to variational definitions of Schatten- p matrix norms and quasi-norms.

Given a matrix $M \in \mathbb{R}^{m \times n}$ and a value of $p > 0$ the Schatten- p matrix norm (for $p \geq 1$) or quasi-norm (for $0 < p < 1$) is notated as $\|M\|_p$ and defined:

$$\|M\|_p = \left(\sum_{i=1}^{\min\{m,n\}} \sigma_i(M)^p \right)^{\frac{1}{p}} \quad (21)$$

where $\sigma_i(M)$ denotes the i^{th} singular of M . This includes many well-known matrix norms, such as the Frobenius norm ($p = 2$), the l_2 induced operator norm (the largest singular value of M for $p = \infty$), and the nuclear norm ($p = 1$). The nuclear norm in particular has received considerable attention in the literature on low-rank matrix recovery, as it is the tightest convex approximation of the rank of a matrix, which allows it to be used as a convex regularizer to induce low-rank solutions. Moreover, if one considers Schatten- p quasi-norms with $0 < p < 1$ (so called because they no longer satisfy the triangle inequality) one achieves an increasingly tighter approximation of the rank of a matrix in the limit as $p \rightarrow 0$, with the downside being that the quasi-norm is no longer convex for $0 < p < 1$.

To show the connection between Schatten- p (quasi)norms and the matrix factorization objective in (11) we will rely on a variational definition of $\|M\|_p$. In particular, the following result can be shown:

Corollary 1. (Adapted from [23]) Given a matrix $M \in \mathbb{R}^{m \times n}$ with $\text{rank}(M) \leq d$ and $L \geq 2$, define matrices $W_L \in \mathbb{R}^{m \times d}$, $W_1 \in \mathbb{R}^{d \times n}$, and $W_l \in \mathbb{R}^{d \times d}$ for $l = 2, \dots, L-1$. Then, we have that

$$\frac{2}{L} \left(\|M\|_{\frac{2}{L}} \right)^{\frac{2}{L}} = \min_{W_L, \dots, W_1} \frac{1}{2} \sum_{l=1}^L \|W_l\|_F^2 \quad \text{s.t.} \quad W_L W_{L-1} \cdots W_2 W_1 = M. \quad (22)$$

The result in (22) implies that if we minimize any matrix factorization model with Frobenius regularization on the matrix factors, then we are effectively minimizing a problem with Schatten- $\frac{2}{L}$ regularization on the product of the W matrices (potentially also with rank constraints on the product if $d < \min\{m, n\}$). To see this explicitly note that the following optimization problems are all equivalent by applying (22):

$$\min_{W_L, \dots, W_1} f(W_L W_{L-1} \cdots W_2 W_1) + \frac{\lambda}{2} \sum_{l=1}^L \|W_l\|_F^2 \quad (23)$$

$$\iff \min_{W_L, \dots, W_1, M} f(M) + \frac{\lambda}{2} \sum_{l=1}^L \|W_l\|_F^2 \quad \text{s.t.} \quad W_L W_{L-1} \cdots W_2 W_1 = M \quad (24)$$

$$\iff \min_M f(M) + \frac{2\lambda}{L} \left(\|M\|_{\frac{2}{L}} \right)^{\frac{2}{L}} \quad \text{s.t.} \quad \text{rank}(M) \leq d. \quad (25)$$

Here the equivalence is in the sense that any global minimizer for the W parameters in (23) will also be a minimizer for (25) with the relation $W_L W_{L-1} \cdots W_2 W_1 = M$, and the rank constraints in (25) arise simply from the fact that in the above equations the rank of M is constrained by parameterizing the W matrices with d -dimensions (if we take $d \geq \min\{m, n\}$ then the rank constraint is irrelevant).

As an example, if we return to the deep matrix factorization problem in (11) we have that the problem is equivalent to finding an approximation of Φ by a matrix with small singular values (and hence low-rank):

$$(11) : \min_{W_L, \dots, W_1} \frac{1}{2} \|W_L \cdots W_1 - \Phi\|_F^2 + \frac{\lambda}{2} \sum_{l=1}^L \|W_l\|_F^2 \iff \quad (26)$$

$$\min_{M: \text{rank}(M) \leq d} \frac{1}{2} \|M - \Phi\|_F^2 + \frac{2\lambda}{L} \left(\|M\|_{\frac{2}{L}} \right)^{\frac{2}{L}} = \min_{M: \text{rank}(M) \leq d} \frac{1}{2} \|M - \Phi\|_F^2 + \frac{2\lambda}{L} \sum_{i=1}^d \sigma_i(M)^{\frac{2}{L}}.$$

If we take the simple example of $L = 2$ (and with d sufficiently large to ignore the rank constraint), then the regularization on M becomes the nuclear norm, and the closed form solution for the optimal M is well-known to be the soft thresholding of the singular values of Φ – i.e., if we let $USV^T = \Phi$ be a singular value

decomposition of Φ , then the optimal value is $M = U(S - \lambda I)_+ V^\top$. As a result, if Φ has any singular values smaller than λ , the recovered solution will also be low rank. Likewise, for deep matrix factorizations ($L > 2$) the singular values of the final recovered M matrix will also be shrunk more aggressively as the depth of the regularization (L) increases.

4.3 Low-Rank Structure from Implicit Regularization

Building on this background we developed above, we now consider the role of the implicit regularization of gradient descent in promoting low-rank structure. In particular, the authors of [24] analyze classification models (i.e., when \mathbf{y} is discrete) trained with gradient descent using 1) exponential family loss functions and 2) models whose predictions are *positively homogeneous* with respect to the model parameters. Specifically, if we notate the network predictions as $\hat{\mathbf{y}} := f_{\Theta}(\mathbf{x})$, the authors consider loss functions that take the form $e^{g(\hat{\mathbf{y}}, \mathbf{y})}$ for functions g that satisfy certain smoothness and monotonicity conditions. Common losses such as the cross-entropy loss and the exponential loss are special cases (see [24] for details). Moreover, the authors assume that the model is positively homogeneous in the model parameters³ – that is there exists $p > 0$ such that for any model input \mathbf{x} , choice of model parameters Θ , and $\alpha \geq 0$ we have $f_{\alpha\Theta}(\mathbf{x}) = \alpha^p f_{\Theta}(\mathbf{x})$. With the two conditions, the authors of [24] then show that if the model perfectly classifies the training data, then the particular solution found by gradient descent will be the maximum margin classifier (that is, gradient descent will find a classifier which perfectly classifies the training data with minimal squared norm on the model parameters).

To better illustrate this general statement, consider the simplified setting of binary classification (i.e., $\mathbf{y} \in \{-1, 1\}$) with a deep linear network trained with the exponential loss,

$$\min_{\Theta} F(\Theta) = \sum_{i=1}^N \exp\{-(\mathbf{W}_L \cdots \mathbf{W}_1 \mathbf{x}_i \cdot \mathbf{y}_i)\}. \quad (27)$$

In this setting, we have that the model predictions are given by $f_{\Theta}(\mathbf{x}) = \mathbf{W}_L \cdots \mathbf{W}_1 \mathbf{x}$ which is clearly positively homogeneous in the model parameters $\Theta = \{\mathbf{W}_L, \dots, \mathbf{W}_1\}$. Also, note that the level-sets for the exponential loss are unbounded, so there is no global minimizer of the loss and the magnitude of the parameters will grow unbounded during the optimization, so as a result it is necessary to consider the direction the parameters converge to by analyzing the normalized parameters $\bar{\Theta} = \frac{\Theta}{\|\Theta\|_F}$, about which the following result can be shown.

Theorem 3. (Informal - adapted from [24]) Consider the following training problem for a deep linear model trained with the exponential loss:

$$\min_{\Theta} F(\Theta) = \sum_{i=1}^N \exp\{-(\mathbf{W}_L \cdots \mathbf{W}_1 \mathbf{x}_i \cdot \mathbf{y}_i)\}. \quad (28)$$

If the model is trained with gradient descent with sufficiently small step-size and at any point during training the model perfectly classifies the data (i.e., $\mathbf{W}_L \cdots \mathbf{W}_1 \mathbf{x}_i \cdot \mathbf{y}_i > 0, \forall i = 1, \dots, n$) then in direction the parameters will converge to a Karush–Kuhn–Tucker (KKT) point of the max-margin classification problem. Specifically, any limit point of the parameter directions $\bar{\Theta} = \frac{\Theta}{\|\Theta\|_F}$ will be a KKT point of the problem:

$$\min_{\Theta} \frac{1}{2} \sum_{l=1}^L \|\mathbf{W}_l\|_F^2 \text{ s.t. } \mathbf{W}_L \cdots \mathbf{W}_1 \mathbf{x}_i \cdot \mathbf{y}_i \geq 1, \forall i = 1, \dots, n \quad (29)$$

That is, the parameter directions $\bar{\Theta}$ found by gradient descent on (27) will be a KKT point of (29) to within a non-negative scaling - namely if Θ_{KKT} is a KKT point of (29), then $\exists \alpha > 0$ such that $\alpha \bar{\Theta} = \Theta_{KKT}$.

Here again, one can note that although there is no explicit regularization on the model parameters, the implicit regularization of the gradient descent dynamics finds a direction of the parameters which is a KKT point the problem in (29) which seeks to find a classifier with minimal l_2 norms on the model parameters

³Recall that deep linear networks are positively homogeneous along with networks that use many common non-linearities, such as ReLU, leaky ReLU, max-pooling, etc.

(the maximum margin classifier)⁴. Note that problems (27) and (29) are both non-convex so we are not guaranteed that gradient descent will find a global minimum in general, just a KKT point.

Now from our discussion above in Section 4.2, recall that adding l_2 regularization to multi-linear model parameters results in low-rank solutions via the variational form of the Schatten-p (quasi)norms. In particular, for a depth L linear model, we can directly apply the result from (22) to the product of the first $L - 1$ layers to see that the problem will be regularized by the Schatten- $\frac{2}{L-1}$ quasi-norm. Namely, if the data can be linearly classified during training, then (in direction) the model parameters will converge to a KKT point of the problem

$$\min_{\mathbf{W}_L, \mathbf{M}} \frac{1}{2} \|\mathbf{W}_L\|_F^2 + \frac{2}{L-1} \left(\|\mathbf{M}\|_{\frac{2}{L-1}} \right)^{\frac{2}{L-1}} \quad \text{s.t. } \mathbf{W}_L \mathbf{M} \mathbf{x}_i \cdot \mathbf{y}_i \geq 1, \forall i = 1, \dots, N. \quad (30)$$

Note that this can be interpreted as first finding a low-rank projection of the data $\mathbf{M} \mathbf{x}$, where \mathbf{M} is regularized to be low-rank via the Schatten- $\frac{2}{L-1}$ quasinorm (assuming $L \geq 3$) and then classifying that low-rank projection via the linear max-margin classifier \mathbf{W}_L .

4.4 Masked Training

Another area where low-rank structure naturally arises in deep learning is when the data representation is *masked* during training. More precisely, one stochastically replaces a portion of the data representation with default values such as zeros or noise, either in the space of the raw data or a latent representation of the data (e.g., in an intermediate layer of a deep network). This paradigm has been widely adopted in modern machine learning, as illustrated in the two examples.

Example 4.1 (Dropout). *One widespread use of masking in deep learning is the Dropout algorithm [25], where at each iteration of training a random subset of the neuron activations is set to zero, while all neurons remain active during inference. This is motivated by the intuition that the induced stochasticity from masking portions of the latent representation would improve robustness and prevent overfitting. The technique has been successfully applied across various neural architectures, including convolutional neural networks (CNNs) for computer vision, recurrent neural networks (RNNs) for sequence modeling, and transformer models for natural language processing [26]. Dropout has also inspired variants that apply different masking strategies, such as DropConnect, which randomly masks weights rather than activations, and Variational Dropout, which learns per-parameter dropout rates through variational inference.*

Example 4.2 (Masked self-supervised learning). *Masked self-supervised training refers to the idea that one randomly replaces a subset of the input with a default value and trains the model to reconstruct the unobserved input from the rest. It has become a fundamental technique in modern language and image modeling. Indeed, language models are trained by learning to predict unobserved text tokens using either the surrounding (BERT [27]) or previous tokens (GPT [28]) in the sequence. The success of this paradigm motivates its extension to image modeling, where the models are trained to reconstruct unobserved image patches from observed ones (MAE [29]). Intuitively, the masking forces the network to learn efficient representations that allows inferring the correlation between the observed and unobserved data.*

To understand the effect of masking in training a network, initial works considered Dropout training in the simplified case of training a matrix factorization model (or equivalently a single hidden layer linear neural network) with the squared loss [30, 31]. In this context, the authors of [30] observe that given a set of training data (\mathbf{X}, \mathbf{Y}) then Dropout training can be viewed as minimizing the following objective:

$$\min_{\mathbf{W}_1, \mathbf{W}_2} \mathbb{E}_{\mathbf{z} \sim \text{i.i.d. Ber}(\mu)} \left\| \mathbf{Y} - \frac{1}{\mu} \mathbf{W}_2 \text{Diag}(\mathbf{z}) \mathbf{W}_1 \mathbf{X} \right\|_F^2. \quad (31)$$

Specifically, \mathbf{z} is a vector of i.i.d. Bernoulli random variables with mean μ , so Dropout training can be viewed as performing Stochastic Gradient Descent (SGD) on this objective by stochastically sampling a vector of \mathbf{z}

⁴The work of [24] also provides similar results for more general settings, such as alternative loss functions and multi-class classification with general positively-homogeneous models, and we refer the reader to [24] for the full technical details.

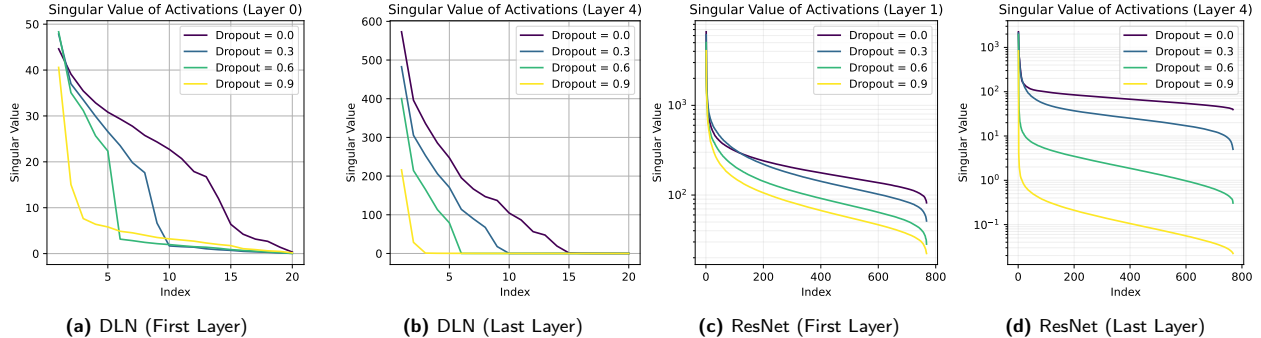


Figure 9: Singular values of activations of the first and last layers in deep architectures from masked training with varying dropout rates $1 - \mu$. Deep Linear Network (DLN) is trained on synthetic data with MSE loss, while ResNet is trained on CIFAR-10 dataset of natural images with cross-entropy loss. As seen, the activations of deep and shallow layers of the trained network exhibit lower numerical rank when the dropout rate used in training is higher.

variables at each iteration of the optimization algorithm (i.e., randomly zeroing out the activations of the associated hidden units). Then, simply expanding the quadratic term and evaluating this expectation leads to an equivalent deterministic regularized problem

$$\min_{\mathbf{W}_1, \mathbf{W}_2} \|\mathbf{Y} - \mathbf{W}_2 \mathbf{W}_1 \mathbf{X}\|_F^2 + \frac{1 - \mu}{\mu} \sum_{i=1}^d \|(\mathbf{W}_2)_{:,i}\|_2^2 \|\mathbf{X}^\top (\mathbf{W}_1)_{i,:}\|_2^2. \quad (32)$$

where one solves the original matrix factorization objective plus a regularization on the d columns of the \mathbf{W}_2 matrix and d rows of the \mathbf{W}_1 matrix. Moreover, again connecting this with the variational form of the nuclear norm described above, the authors of [30] and [31] establish that the above problem is equivalent to a nuclear norm regularized problem. In particular, the following problems are equivalent provided that d , the number of columns/rows in $(\mathbf{W}_2, \mathbf{W}_1)$ respectively, is sufficiently large:

$$\min_{\mathbf{W}_1, \mathbf{W}_2} \mathbb{E}_{\mathbf{z} \sim \text{i.i.d. Ber}(\mu)} \left\| \mathbf{Y} - \frac{1}{\mu} \mathbf{W}_2 \text{Diag}(\mathbf{z}) \mathbf{W}_1 \mathbf{X} \right\|_F^2 \iff \min_{\mathbf{Z}} \|\mathbf{Y} - \mathbf{Z}\|_F^2 + \frac{1 - \mu}{\mu} \|\mathbf{Z}\|_*^2, \quad (33)$$

where the equivalence is in the sense that optimal solutions $(\mathbf{W}_1^*, \mathbf{W}_2^*)$ and \mathbf{Z}^* will satisfy $\mathbf{Z}^* = \mathbf{W}_2^* \mathbf{W}_1^* \mathbf{X}$. From this, one can observe that the use of Dropout training induces low-rank solutions due to the low-rank promoting properties of the nuclear norm.

Moreover, this work was then later extended to provide a similar characterization for Dropout applied to deep linear networks [32] and with Dropout applied to a final layer of a non-linear network with potentially different statistics (i.e., non-Bernoulli) on the Dropout variables [33]. In all cases, Dropout is shown to induce low-rank solutions, and the authors of [34] further show that this also constrains statistical model complexity measures of the network, such as the Rademacher complexity.

We conduct experiments to visualize the effect of dropout on the rank of the activations. We begin with the regime covered by the theoretical results reviewed above (i.e., last layer of deep linear network trained by MSE loss), and then explore cases not yet modeled by existing theory (i.e., shallower layers, non-linear networks such as multi-layer perceptrons (MLP) and residual network (ResNet), and cross entropy loss). Experiment setups are detailed in Appendix A in the supplementary materials. As seen in Figure 9, the activations of both deep and shallow layers of the trained network exhibit lower numerical rank when the dropout rate used in training is higher. Figure 2 further shows that the activations of the layers gradually become low-rank as masked training proceeds.

More recently, other variants of masking data or latent representations of data have received considerable attention in applications of Masked Autoencoders (MAEs) and Masked Language Modelling (MLM). In this setting, empirical evidence has suggested that the features learned by MAEs and MLMs are approximately low-rank, suggesting that a potential general property of masking is to induce low-rank structures, although it remains an open direction for future work to theoretically establish this rigorously. For instance, the authors of [35] observe empirically that the features of MAEs at convergence have lower effective rank than at

random initialization. They provide a theoretical connection between MAEs and contrastive learning, albeit how this relates to the low-rank features remains unclear. Interestingly, the work of [36] further provides empirical evidence that a lower effective rank on the features learned by a variant of MAEs (achieved by re-weighting the residual connections in the architecture) leads to higher the linear probing accuracy. On the other hand, the work of [37] shows that on a pretrained MLM, inputs with masking empirically lead to features of lower effective rank than the same inputs without masking at all, with the difference of ranks being larger as the layer goes deeper. They prove that the features of the unmasked inputs must be rank-deficient at some layer, though it remains an open question to theoretically guarantee how small the rank can be.

5 Open Questions and Future Directions

In this paper, we explored the role of low-rank structure in the training and adaptation of deep learning models. We reviewed recent advances in understanding low-rank dynamics during training and highlighted how implicit low-rank structures can reduce the number of required data samples for model learning. Additionally, we discussed methods such as LoRA that optimize large-scale models more efficiently by using low-rank approximations of the weight matrices. However, low-rank structures are also relevant to other important challenges in deep learning, such as improving model generalization and interpretability. In this section, we highlight some compelling open questions and propose promising future directions for research, with the aim of motivating more research in these crucial areas.

One promising direction is to extend the theoretical study of low-rank structures from deep linear networks to deep nonlinear networks. For instance, in Section 3.1, we demonstrated that gradient updates in deep linear networks occur within a low-rank subspace. Although the Galore work in Section 3.3 provides some insights into the emergence of low-rank gradients in deep nonlinear networks, these findings depend on relatively restrictive assumptions, such as network reversibility, specific loss functions, and small batch sizes. Extending the analysis to more practical settings would provide better theoretical justification for employing low-rank training. Another promising direction lies in improving model interpretability through low-rank structures, which could offer simpler and more human-understandable explanations of the learned features or transformations in complex architectures, such as diffusion models and large language models. For example, the interplay between low-rank structures and phenomena like neural collapse [38, 39] in supervised learning offers fertile ground for advancing our understanding of these models’ underlying mechanics. Additionally, leveraging low-rank approximations to improve generative AI efficiency has gained traction, particularly in the context of LLMs, where self-attention maps often exhibit low-rank characteristics. This observation has inspired techniques that approximate self-attention matrices to reduce computational complexity while maintaining performance.

Acknowledgment

LB, CY, SK, and PW acknowledge NSF CAREER CCF-1845076, NSF CCF-2331590. QQ, CY, SK, and PW acknowledge NSF CAREER CCF-2143904, NSF IIS 2312842, NSF IIS 2402950, and ONR N00014-22-1-2529. LB also acknowledges the U-M Crosby Award, Intel Early Career Award, and the IAS Charles Simonyi Endowment. ZW acknowledges NSF Awards 2145346 (CAREER), 02133861 (DMS), 2113904 (CCSS), and the NSF AI Institute for Foundations of Machine Learning (IFML). TD and BDH acknowledge NSF 2212457. The authors would like to thank Zekai Zhang (University of Michigan) for his insights into the relationship between ReLoRA and GaLore.

References

- [1] Soo Min Kwon, Zekai Zhang, Dogyoon Song, Laura Balzano, and Qing Qu. Efficient low-dimensional compression of overparameterized models. In *Proceedings of The 27th International Conference on Artificial Intelligence and Statistics*, volume 238 of *Proceedings of Machine Learning Research*, pages 1009–1017. PMLR, 2024.

- [2] Edward J Hu, Phillip Wallis, Zeyuan Allen-Zhu, Yuanzhi Li, Shean Wang, Lu Wang, Weizhu Chen, et al. LoRA: Low-rank adaptation of large language models. In *International Conference on Learning Representations*, 2021.
- [3] Aixin Liu, Bei Feng, Bing Xue, Bingxuan Wang, Bochao Wu, Chengda Lu, Chenggang Zhao, Chengqi Deng, Chenyu Zhang, Chong Ruan, et al. Deepseek-v3 technical report. *arXiv preprint arXiv:2412.19437*, 2024.
- [4] Rahul Parhi and Robert D Nowak. Deep learning meets sparse regularization: A signal processing perspective. *IEEE Signal Processing Magazine*, 40(6):63–74, 2023.
- [5] Andrew M Saxe, James L McClelland, and Surya Ganguli. A mathematical theory of semantic development in deep neural networks. *Proceedings of the National Academy of Sciences*, 116(23):11537–11546, 2019.
- [6] Peng Wang, Xiao Li, Can Yaras, Zhihui Zhu, Laura Balzano, Wei Hu, and Qing Qu. Understanding deep representation learning via layerwise feature compression and discrimination. *arXiv preprint arXiv:2311.02960*, 2023.
- [7] Gilbert W Stewart. On the early history of the singular value decomposition. *SIAM Review*, 35(4): 551–566, 1993.
- [8] Can Yaras, Peng Wang, Laura Balzano, and Qing Qu. Compressible dynamics in deep overparameterized low-rank learning & adaptation. In *International Conference on Machine Learning*, pages 56946–56965. PMLR, 2024.
- [9] A Saxe, J McClelland, and S Ganguli. Exact solutions to the nonlinear dynamics of learning in deep linear neural networks. In *International Conference on Learning Representations*, 2014.
- [10] Sanjeev Arora, Nadav Cohen, Wei Hu, and Yuping Luo. Implicit regularization in deep matrix factorization. *Advances in Neural Information Processing Systems*, 32, 2019.
- [11] Ziwei Ji and Matus Telgarsky. Gradient descent aligns the layers of deep linear networks. In *International Conference on Learning Representations*, 2019.
- [12] Zhiyuan Li, Yuping Luo, and Kaifeng Lyu. Towards resolving the implicit bias of gradient descent for matrix factorization: Greedy low-rank learning. In *International Conference on Learning Representations*, 2021.
- [13] Soufiane Hayou, Nikhil Ghosh, and Bin Yu. LoRA+: Efficient low rank adaptation of large models. In *International Conference on Machine Learning*, pages 17783–17806. PMLR, 2024.
- [14] Jui-Nan Yen, Si Si, Zhao Meng, Felix Yu, Sai Surya Duvvuri, Inderjit S Dhillon, Cho-Jui Hsieh, and Sanjiv Kumar. LoRA done RITE: Robust invariant transformation equilibration for loRA optimization. In *The Thirteenth International Conference on Learning Representations*, 2025.
- [15] Qingru Zhang, Minshuo Chen, Alexander Bukharin, Pengcheng He, Yu Cheng, Weizhu Chen, and Tuo Zhao. Adaptive budget allocation for parameter-efficient fine-tuning. In *The Eleventh International Conference on Learning Representations*, 2023.
- [16] Qingru Zhang, Minshuo Chen, Alexander Bukharin, Pengcheng He, Yu Cheng, Weizhu Chen, and Tuo Zhao. Adaptive budget allocation for parameter-efficient fine-tuning. In *The Eleventh International Conference on Learning Representations*, 2022.
- [17] Jacob Devlin, Ming-Wei Chang, Kenton Lee, and Kristina Toutanova. BERT: Pre-training of deep bidirectional transformers for language understanding. In Jill Burstein, Christy Doran, and Thamar Solorio, editors, *Proceedings of the 2019 Conference of the North American Chapter of the Association for Computational Linguistics: Human Language Technologies, Volume 1 (Long and Short Papers)*, pages 4171–4186, Minneapolis, Minnesota, June 2019. Association for Computational Linguistics. doi: 10.18653/v1/N19-1423. URL <https://aclanthology.org/N19-1423/>.

- [18] Daniel Cer, Mona Diab, Eneko Agirre, Iñigo Lopez-Gazpio, and Lucia Specia. SemEval-2017 task 1: Semantic textual similarity multilingual and crosslingual focused evaluation. In Steven Bethard, Marine Carpuat, Marianna Apidianaki, Saif M. Mohammad, Daniel Cer, and David Jurgen, editors, *Proceedings of the 11th International Workshop on Semantic Evaluation (SemEval-2017)*, pages 1–14, Vancouver, Canada, August 2017. Association for Computational Linguistics. doi: 10.18653/v1/S17-2001. URL <https://aclanthology.org/S17-2001/>.
- [19] Vladislav Lialin, Sherin Muckatira, Namrata Shivagunde, and Anna Rumshisky. ReloRA: High-rank training through low-rank updates. In *The Twelfth International Conference on Learning Representations*, 2024.
- [20] Jiawei Zhao, Zhenyu Zhang, Beidi Chen, Zhangyang Wang, Anima Anandkumar, and Yuandong Tian. Galore: Memory-efficient llm training by gradient low-rank projection. In *International Conference on Machine Learning*, pages 61121–61143. PMLR, 2024.
- [21] Ajay Jaiswal, Lu Yin, Zhenyu Zhang, Shiwei Liu, Jiawei Zhao, Yuandong Tian, and Zhangyang Wang. From galore to welore: How low-rank weights non-uniformly emerge from low-rank gradients. *arXiv preprint arXiv:2407.11239*, 2024.
- [22] Yehonathan Refael, Jonathan Svirsky, Boris Shustin, Wasim Huleihel, and Ofir Lindenbaum. Adarankgrad: Adaptive gradient rank and moments for memory-efficient LLMs training and fine-tuning. In *The Thirteenth International Conference on Learning Representations*, 2025.
- [23] Fanhua Shang, Yuanyuan Liu, Fanjie Shang, Hongying Liu, Lin Kong, and Licheng Jiao. A unified scalable equivalent formulation for Schatten quasi-norms. *Mathematics*, 8(8):1325, 2020.
- [24] Kaifeng Lyu and Jian Li. Gradient descent maximizes the margin of homogeneous neural networks. *The Eighth International Conference on Learning Representations*, 2020.
- [25] Nitish Srivastava, Geoffrey Hinton, Alex Krizhevsky, Ilya Sutskever, and Ruslan Salakhutdinov. Dropout: a simple way to prevent neural networks from overfitting. *Journal of Machine Learning Research*, 15(56):1929–1958, 2014.
- [26] Ashish Vaswani, Noam Shazeer, Niki Parmar, Jakob Uszkoreit, Llion Jones, Aidan N Gomez, Łukasz Kaiser, and Illia Polosukhin. Attention is all you need. *Advances in Neural Information Processing Systems*, 30, 2017.
- [27] Jacob Devlin, Ming-Wei Chang, Kenton Lee, and Kristina Toutanova. BERT: Pre-training of deep bidirectional transformers for language understanding. In *Proceedings of the 2019 Conference of the North American Chapter of the Association for Computational Linguistics: Human Language Technologies, Volume 1 (Long and Short Papers)*, pages 4171–4186, Minneapolis, Minnesota, June 2019. Association for Computational Linguistics. doi: 10.18653/v1/N19-1423.
- [28] Alec Radford, Karthik Narasimhan, Tim Salimans, Ilya Sutskever, and others. Improving language understanding by generative pre-training. 2018. Publisher: San Francisco, CA, USA.
- [29] Kaiming He, Xinlei Chen, Saining Xie, Yanghao Li, Piotr Dollár, and Ross Girshick. Masked autoencoders are scalable vision learners. In *Proceedings of the IEEE/CVF Conference on Computer Vision and Pattern Recognition*, pages 16000–16009, 2022.
- [30] Jacopo Cavazza, Pietro Morerio, Benjamin Haeffele, Connor Lane, Vittorio Murino, and Rene Vidal. Dropout as a low-rank regularizer for matrix factorization. In *International Conference on Artificial Intelligence and Statistics*, pages 435–444. PMLR, 2018.
- [31] Poorya Mianjy, Raman Arora, and Rene Vidal. On the implicit bias of dropout. In *International Conference on Machine Learning*, pages 3540–3548. PMLR, 2018.
- [32] Poorya Mianjy and Raman Arora. On dropout and nuclear norm regularization. In *International Conference on Machine Learning*, pages 4575–4584. PMLR, 2019.

- [33] Ambar Pal, Connor Lane, René Vidal, and Benjamin D Haeffele. On the regularization properties of structured dropout. In *Proceedings of the IEEE/CVF Conference on Computer Cision and Pattern Recognition*, pages 7671–7679, 2020.
- [34] Raman Arora, Peter Bartlett, Poorya Mianjy, and Nathan Srebro. Dropout: Explicit forms and capacity control. In *International Conference on Machine Learning*, pages 351–361. PMLR, 2021.
- [35] Qi Zhang, Yifei Wang, and Yisen Wang. How mask matters: Towards theoretical understandings of masked autoencoders. *Advances in Neural Information Processing Systems*, 35:27127–27139, 2022.
- [36] Xiao Zhang, Ruoxi Jiang, William Gao, Rebecca Willett, and Michael Maire. Residual connections harm generative representation learning, January 2025. arXiv:2404.10947 [cs].
- [37] Yu Meng, Jitin Krishnan, Sinong Wang, Qifan Wang, Yuning Mao, Han Fang, Marjan Ghazvininejad, Jiawei Han, and Luke Zettlemoyer. Representation deficiency in masked language modeling. In *The Twelfth International Conference on Learning Representations*, 2024.
- [38] Vardan Papyan, XY Han, and David L Donoho. Prevalence of neural collapse during the terminal phase of deep learning training. *PNAS*, 117(40):24652–24663, 2020.
- [39] Zhihui Zhu, Tianyu Ding, Jinxin Zhou, Xiao Li, Chong You, Jeremias Sulam, and Qing Qu. A geometric analysis of neural collapse with unconstrained features. *Advances in Neural Information Processing Systems*, 34:29820–29834, 2021.
- [40] Alexey Dosovitskiy, Lucas Beyer, Alexander Kolesnikov, Dirk Weissenborn, Xiaohua Zhai, Thomas Unterthiner, Mostafa Dehghani, Matthias Minderer, Georg Heigold, Sylvain Gelly, Jakob Uszkoreit, and Neil Houlsby. An image is worth 16x16 words: Transformers for image recognition at scale. In *9th International Conference on Learning Representations, ICLR 2021, Virtual Event, Austria, May 3-7, 2021*, 2021. URL <https://openreview.net/forum?id=YicbFdNTTy>.
- [41] Can Yaras, Peng Wang, Wei Hu, Zhihui Zhu, Laura Balzano, and Qing Qu. The law of parsimony in gradient descent for learning deep linear networks. *arXiv preprint arXiv:2306.01154*, 2023.

A Experiment Details

Low-Rank Structure at Every Iteration of Gradient Dynamics (§3) For Figure 1, the linear network and MLP were trained on MNIST and the VGG-16 and ViT were trained on CIFAR-10. We observe the change in singular values of the penultimate weight matrix for DLNs, MLPs, VGG, and ViT-B. We train the DLN starting from orthogonal initialization using SGD with learning rate 0.01 and a batch size of 128. All of the nonlinear networks were initialized using random uniform initialization. For MLP, we train using the same parameters as the DLN. For VGG, we use batch size 128 with learning rate 0.05, weight decay parameter 5×10^{-4} , momentum 0.9, and step size scheduler with cosine annealing. Lastly, for ViT-B, we train using ADAM with a batch size of 512 and learning rate 10^{-5} with cosine annealing. The ViT-B architecture is the same as the one presented by Dosovitskiy et al. [40]. Figures 8 and 10 follow the same training procedure for the ViT above.

Table 1: Summary of setups of experiments in §4.

Experiment	Architecture	Dataset	Loss Function	Batch Size
1	Deep Linear Network	Synthetic	MSE	1024
2	Multi-Layer Perceptron	Synthetic	MSE	1024
3	ResNet	CIFAR-10	Cross-Entropy	768

Low-Rank Structure at the Global Minimum of Objective Functions (§4) We design the experiments to investigate the impact of dropout on the singular values (or effective rank) of activations in neural networks, where we progressively extend theoretical predictions to practical scenarios. Table 1 summarizes the architecture, dataset, and loss function of each experiment. *Synthetic Data Generation:* For Experiments 1 and 2, we generate synthetic datasets. Inputs $x \in \mathbb{R}^{20}$ are drawn from a standard Gaussian distribution. The corresponding outputs $y \in \mathbb{R}^{20}$ are generated via a linear transformation with a fixed matrix of rank 15. This design ensures outputs lie in a 15-dimensional subspace of \mathbb{R}^{20} . *Network Architecture and Loss Function:* In Experiment 1, we utilize a deep linear network comprising three linear layers with dimensions 20-20-20, separated by dropout layers, and optimized using mean squared error (MSE) loss. Experiment 2 introduces nonlinearities into the network by inserting ReLU activations after each intermediate linear layer, except for the output layer, thus forming a multilayer perceptron (MLP). Experiment 3 adopts a practical setting using a ResNet architecture with residual blocks arranged in a 2-2-2-2 configuration, channel dimensions starting at 64 and doubling progressively (64, 128, 256, 512). This network is trained on the CIFAR-10 dataset, employing cross-entropy loss to reflect a realistic classification scenario. In all three experiments an SGD optimizer is used with a learning rate of 10^{-2} and no momentum whatsoever.

B Complexity for Forward and Backward Pass

Almost all of the computational cost (and a majority of the memory cost) in training deep networks involves dense linear layers of the form $\mathbf{Y} = \mathbf{W}\mathbf{X}$, where $\mathbf{X} \in \mathbb{R}^{d \times n}$ are the input activations (i.e., the batch of hidden feature vectors after passing through a nonlinearity from a previous layer), $\mathbf{Y} \in \mathbb{R}^{d \times n}$ are output activations, and $\mathbf{W} \in \mathbb{R}^{d \times d}$ is a weight matrix. During forward propagation, we receive input activations \mathbf{X} from the previous layer, compute \mathbf{Y} with $\Theta(nd^2)$ operations, which is passed to the subsequent layer, and store \mathbf{X} for backpropagation. During backpropagation, we receive the output activation gradient $\nabla_{\mathbf{Y}}\mathcal{L}$ with respect to some loss \mathcal{L} from the subsequent layer, which we use to compute the weight matrix gradient $\nabla_{\mathbf{W}}\mathcal{L} = \nabla_{\mathbf{Y}}\mathcal{L} \cdot \mathbf{X}^{\top}$ with $\Theta(nd^2)$ operations, and also the input activation gradient $\nabla_{\mathbf{X}}\mathcal{L} = \mathbf{W}^{\top} \cdot \nabla_{\mathbf{Y}}\mathcal{L}$ with $\Theta(nd^2)$ operations, with the latter passed to the preceding layer. Overall, for each layer we have $3 \times \Theta(nd^2)$ operations. From a memory standpoint, for each layer we need to store $\Theta(d^2)$ for the weight matrix (and its optimizer state which is $2 \times$ the size of weight matrix for Adam), as well as $\Theta(nd)$ for input activations.

There are some “tricks” that can be (and are) employed in practice to save memory, which slightly change the above setting. One example is “gradient checkpointing”, where we only store input activations at certain layers (called checkpoints), which we can use to recompute a given layer’s input activations for backpropagation. We are effectively trading memory for compute – if we only store every other layer’s input

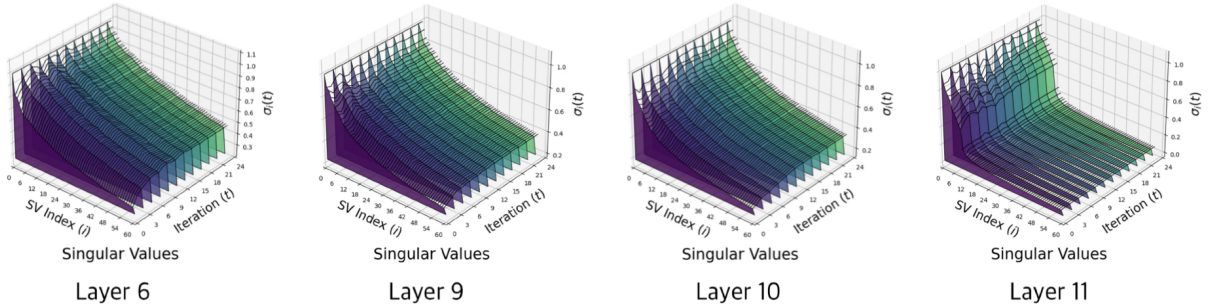


Figure 10: Singular values across layers of the ViT of the value weight matrix. Similar to the observations in Figure 8, the value matrices corresponding to the Transformer of the shallower layers do not have a low-rank structure, and the low-rank structure emerges in the deeper layers.

activations, we halve the memory requirements for these, while introducing another matrix multiplication for every other layer.

C Low-Rank Gradient Dynamics with a Wide Target

In Section 3.1, we consider deep matrix factorization where the target matrix Φ has d rows. In a more standard regression or classification setting for $\Phi = \mathbf{Y}\mathbf{X}^\top(\mathbf{X}\mathbf{X}^\top)^{-1}$, we really have k rows, where k is the label dimension (e.g., corresponding to k classes). In most cases, $k \ll d$, i.e., we have many fewer output coordinates than the network width or input dimensionality. To address this case, suppose $\Phi \in \mathbb{R}^{k \times d}$, where $r = k \ll d$ is the rank of Φ . We modify \mathbf{W}_L in Equation (11) to be $\mathbf{W}_L \in \mathbb{R}^{k \times d}$ to match dimensions. Then, a very similar result to Theorem 2 can be shown, with the only differences being that (1) the decomposition holds for all layers $l \in [L - 1]$, i.e., excluding layer L , and (2) $\rho_l^{(t)} = \epsilon_l(1 - \eta\lambda)^t$ exactly. This result and its proof are found in [41].

D Low-Rank Training

This section of the appendix presents additional results that complement the low-rank training analysis in Section 3.3. Specifically, we include the following:

- *An illustration of rank differences in value matrices of ViT.* The difference of low-rank structures across the layers of value matrices in ViT models are shown in Figure 10.
- *Algorithm pipeline of GaLore.* Additionally, we provide more details of GaLore method based upon Adam optimizer in Algorithm 1.
- *Equivalence of GaLore and ReLoRA with full rank gradient initialization.* Finally, here we include proof of the equivalence of ReLoRA [19] and GaLore [20] detailed in the following.

Theorem 4 (GD-GaLore and GD-ReLoRA are equivalent with full rank gradient initialization). *Initialize GD-GaLore from [20] and GD-ReLoRA from [19] with the same initial point. In particular, initialize the \mathbf{B} matrix in ReLoRA with the SVD of full gradients (rather than random Gaussian) and fix it. Then, the weight updates for each algorithm are identical at every iteration.*

Proof. We prove this by induction. We use the notation from the GaLore algorithm and denote quantities related to GD-ReLoRA with a prime (e.g., $\mathbf{W}^{(t)^\prime}$).

Induction Hypothesis

Assume that GD-GaLore and GD-ReLoRA start with the same initialization and produce the same result at iteration $t - 1$:

$$\begin{cases} \mathbf{W}^{(t-1)} = \mathbf{W}^{(t-1)'} \\ \mathbf{P}^{(t-1)} = \mathbf{B}^{(t-1)}. \end{cases}$$

where

$$\begin{aligned} \mathbf{W}^{(k)'} &:= \mathbf{W}^{(0)} + \mathbf{B}^{(0)} \mathbf{A}^{(0)} + \mathbf{B}^{(T)} \mathbf{A}^{(T)} + \dots + \mathbf{B}^{(\lfloor (k-1)/T \rfloor T)} \mathbf{A}^{(\lfloor (k-1)/T \rfloor T)} + \mathbf{B}^{(k)} \mathbf{A}^{(k)} \\ &:= \mathbf{W}^{(\lfloor (k-1)/T \rfloor T)} + \mathbf{B}^{(k)} \mathbf{A}^{(k)} \end{aligned}$$

is the k -th iterate of GD-ReLoRA.

Case 1: $t \bmod T \neq 0$

For GD-GaLore, using the update rule:

$$\begin{aligned} \mathbf{G}^{(t)} &= \nabla_{\mathbf{W}} \phi(\mathbf{W}^{(t-1)}), \mathbf{P}^{(t)} = \mathbf{P}^{(t-1)}, \\ \mathbf{R}^{(t)} &= \mathbf{P}^{(t)\top} \mathbf{G}^{(t)}, \tilde{\mathbf{G}}_t = \mathbf{P}^{(t)} \mathbf{G}^{(t)}, \\ \mathbf{W}^{(t)} &= \mathbf{W}^{(t-1)} - \eta \tilde{\mathbf{G}}_t = \mathbf{W}^{(t-1)} - \eta \mathbf{P}^{(t)} \mathbf{P}^{(t)\top} \nabla_{\mathbf{W}} \phi(\mathbf{W}^{(t-1)}). \end{aligned}$$

For GD-ReLoRA, applying the update rule:

$$\begin{aligned} \mathbf{A}^{(t)} &= \mathbf{A}^{(t-1)} - \nabla_{\mathbf{A}} \phi(\mathbf{W}^{(\lfloor (t-2)/T \rfloor T)} + \mathbf{B}^{(t-1)} \mathbf{A}^{(t-1)}), \mathbf{B}^{(t)} = \mathbf{B}^{(t-1)}, \\ \mathbf{W}^{(t)'} &= \mathbf{W}^{(t-1)'} + \mathbf{B}^{(t)} \mathbf{A}^{(t)} - \mathbf{B}^{(t-1)} \mathbf{A}^{(t-1)}, \\ &= \mathbf{W}^{(t-1)'} - \eta \mathbf{B}^{(t)} \mathbf{B}^{(t)\top} \nabla_{\mathbf{W}} \phi(\mathbf{W}^{(t-1)'}). \end{aligned}$$

where we leverage the chain rule $\nabla_{\mathbf{A}} \phi(\mathbf{W}^{(\lfloor (t-2)/T \rfloor T)} + \mathbf{B}^{(t-1)} \mathbf{A}^{(t-1)}) = \mathbf{B}^{(t-1)\top} \nabla_{\mathbf{W}} \phi(\mathbf{W}^{(t-1)'})$.
By the induction hypothesis:

$$\begin{aligned} \mathbf{W}^{(t)'} &= \mathbf{W}^{(t-1)'} - \eta \mathbf{B}^{(t)} \mathbf{B}^{(t)\top} \nabla_{\mathbf{W}} \phi(\mathbf{W}^{(t-1)'}) \\ &= \mathbf{W}^{(t-1)} - \eta \mathbf{P}^{(t)} \mathbf{P}^{(t)\top} \nabla_{\mathbf{W}} \phi(\mathbf{W}^{(t-1)}) = \mathbf{W}^{(t)}. \end{aligned}$$

Thus, the claim holds for $t \bmod T \neq 0$.

Case 2: $t \bmod T = 0$

Now we consider the case where we need to reinitialize $\mathbf{P}^{(t)}$ and $\mathbf{B}^{(t)}, \mathbf{A}^{(t)}$.
For GD-GaLore, we use the SVD of the full gradient as a projection:

$$\begin{aligned} \mathbf{G}^{(t)} &= \nabla_{\mathbf{W}} \phi(\mathbf{W}^{(t-1)}), [\mathbf{U}, \mathbf{\Sigma}, \mathbf{V}] = \text{SVD}(\mathbf{G}^{(t)}), \\ \mathbf{P}^{(t)} &= \mathbf{U}[:, : r], \mathbf{W}^{(t)} = \mathbf{W}^{(t-1)} - \eta \mathbf{P}^{(t)} \mathbf{P}^{(t)\top} \mathbf{G}^{(t)}. \end{aligned}$$

For GD-ReLoRA, we reinitialize $\mathbf{B}^{(t)}$ using the SVD of the gradient and set $\mathbf{A}^{(t)}$ to zero:

$$\begin{aligned} \mathbf{G}^{(t)'} &= \nabla_{\mathbf{W}} \phi(\mathbf{W}^{(t-1)'}), [\mathbf{U}', \mathbf{\Sigma}', \mathbf{V}'] = \text{SVD}(\mathbf{G}^{(t)'}), \\ \mathbf{B}^{(t)} &= \mathbf{U}'[:, : r], \mathbf{A}^{(t)\text{init}} = 0, \mathbf{W}^{(t)'\text{init}} = \mathbf{W}^{(t-1)'} + \mathbf{B}^{(t)} \mathbf{A}^{(t)\text{init}}, \\ \mathbf{A}^{(t)} &= \mathbf{A}^{(t)\text{init}} - \eta \nabla_{\mathbf{A}} \phi(\mathbf{W}^{(t)'\text{init}}), \\ \mathbf{W}^{(t)'} &= \mathbf{W}^{(t)'\text{init}} + \mathbf{B}^{(t)} \mathbf{A}^{(t)} - \mathbf{B}^{(t)} \mathbf{A}^{(t)\text{init}}, \\ &= \mathbf{W}^{(t-1)'} - \eta \mathbf{B}^{(t)} \mathbf{B}^{(t)\top} \nabla_{\mathbf{W}} \phi(\mathbf{W}^{(t-1)'}). \end{aligned}$$

Algorithm 1 Adam with GaLore (reprinted from [20])

Input: A layer weight matrix $\mathbf{W} \in \mathbb{R}^{m \times n}$ with $m \leq n$. Step size η , scale factor α , decay rates β_1, β_2 , rank r , subspace change frequency T .
Initialize first-order moment $\mathbf{M}_0 \in \mathbb{R}^{n \times r} \leftarrow 0$
Initialize second-order moment $\mathbf{V}_0 \in \mathbb{R}^{n \times r} \leftarrow 0$
Initialize step $t \leftarrow 0$
repeat
 $\mathbf{G}_t \in \mathbb{R}^{m \times n} \leftarrow -\nabla_{\mathbf{W}} \phi_t(\mathbf{W}_t)$ {Should be $\nabla_{\mathbf{W}} \phi_t(\mathbf{W}_{t-1})$?}
 if $t \bmod T = 0$ **then**
 $\mathbf{U}, \mathbf{S}, \mathbf{V} \leftarrow \text{SVD}(\mathbf{G}_t)$
 $\mathbf{P}_t \leftarrow \mathbf{U}[:, :r]$ {Initialize left projector as $m \leq n$ }
 else
 $\mathbf{P}_t \leftarrow \mathbf{P}_{t-1}$ {Reuse the previous projector}
 end if
 $\mathbf{R}_t \leftarrow \mathbf{P}_t^\top \mathbf{G}_t$ {Project gradient into compact space}

 update(\mathbf{R}_t) **by Adam**
 $\mathbf{M}_t \leftarrow \beta_1 \cdot \mathbf{M}_{t-1} + (1 - \beta_1) \cdot \mathbf{R}_t$
 $\mathbf{V}_t \leftarrow \beta_2 \cdot \mathbf{V}_{t-1} + (1 - \beta_2) \cdot \mathbf{R}_t^2$
 $\hat{\mathbf{M}}_t \leftarrow \mathbf{M}_t / (1 - \beta_1^t)$
 $\hat{\mathbf{V}}_t \leftarrow \mathbf{V}_t / (1 - \beta_2^t)$
 $\mathbf{N}_t \leftarrow \hat{\mathbf{M}}_t / (\sqrt{\hat{\mathbf{V}}_t} + \epsilon)$

 $\tilde{\mathbf{G}}_t \leftarrow \alpha \cdot \mathbf{P}_t \mathbf{N}_t$ {Project back to original space}
 $\mathbf{W}_t \leftarrow \mathbf{W}_{t-1} + \eta \cdot \tilde{\mathbf{G}}_t$
 $t \leftarrow t + 1$
until convergence criteria met
return \mathbf{W}_t

Applying the induction hypothesis:

$$\begin{aligned} \mathbf{W}^{(t)'} &= \mathbf{W}^{(t-1)'} - \eta \mathbf{B}^{(t)} \mathbf{B}^{(t)\top} \nabla_{\mathbf{W}} \phi(\mathbf{W}^{(t-1)'}) \\ &= \mathbf{W}^{(t-1)} - \eta \mathbf{P}^{(t)} \mathbf{P}^{(t)\top} \nabla_{\mathbf{W}} \phi(\mathbf{W}^{(t-1)}) = \mathbf{W}^{(t)}. \end{aligned}$$

Since Case 2 also serves as the base case, the proof is complete. □

Remarks:

- This theorem shows that, due to the chain rule, we do not need to compute the full gradient first; instead, we can update the low-rank approximation directly.
- However, we still need to modify GD-ReLoRA by reinitializing \mathbf{B}_t with the SVD of the full gradient every T iterations. This is significantly cheaper than computing the full gradient at every step.
- The proof extends naturally to Adam-GaLore and Adam-ReLoRA, leading to the same conclusion.